Structure Formation from Cosmic Strings

Francis Duplessis

Department of Physics
McGill University
Montréal, Québec
Canada

A Thesis submitted to
McGill University
in partial fulfillment of the requirements for the degree of
Master of Science

© Francis Duplessis, 2013

Contents

List of Figures

Abstract

The search for cosmic strings has been of renewed interest with the advent of precision cosmology. In this thesis we discuss the possibility of observing cosmic strings through their signature in the large scale structure. We review the standard picture of structure formation caused by primordial fluctuations in the matter density and introduce the notion of cosmic strings while presenting how they would act as early seeds for structure formation. We also discuss previous work that studied structures formed from cosmic string loops and the recent result that these could allow for observational effects by giving rise to significant star formation at early times. Finally we give a quantitative description of the nonlinear matter density fluctuations that can form from a scaling network of cosmic string wakes. Specifically, we compute the distribution of dark matter halos. These halos would possess strong correlations in position space that should have survived until today. We also discuss the challenges involved in their detection due to their small size and the complex dynamics of their formation.

Abrégé

L'intérêt pour la recherche de cordes cosmiques c'est récemment renouvelé avec l'arrivée de nouvelles technologies permettant d'étudier la cosmologie avec grande précision. Dans cette thèse, nous discutons de la possibilité d'observer ces cordes cosmiques par leur effet sur les structures à grande échelle de l'univers. Nous présentons le savoir standard associé à la formation de structure causée par des fluctuations primordiales dans la densité de matière. Par la suite, nous expliquons la notion de cordes cosmiques et leur effet catalyseur sur la croissance de structure. Nous discutons également des travaux antérieurs qui ont été effectués sur les structures former par les cordes cosmiques bouclées. Ces travaux démontrent que ces structures peuvent potentiellement générer des étoiles très tôt dans l'histoire de l'univers, cela causerait des effets observables. Finalement, nous donnons une description quantitative des fluctuations de densité non-linéaire causée dans le sillage de longues cordes cosmiques. Spécifiquement, nous calculons la distribution des halos de matière noire. Ces halos posséderaient de fortes corrélations spatial qui devrait avoir survécues jusqu'à aujourd'hui. Nous discutons aussi des obstacles, dûs à leurs petites masses et aux dynamiques complexes de leur formation, auxquels nous devrons surmonter en essayant de détecter les signaux de ces halos.

Acknowledgment

I wish to thank my supervisor Robert Brandenberger for being always available to discuss and put me back on the right track when I strayed off. His valuable comments on the draft of this thesis were also very helpful.

I am also grateful to the McGill HEP group for insuring a stimulating environment through the weekly Journal clubs, seminars, lunch breaks and a faculty that was always very patient and friendly. Moreover the HEP group had the chance of having amazing postdocs such as: Yifu Cai, Alejandra Castro, Joshua Lapan, Zuowei Liu, Pat Scott and Yi Wang. They took a generous amount of their time to teach, and work with, graduate students. This allowed us to learn a great deal of physics.

During the completion of this work I had the pleasure of being surrounded by colorful colleagues. They gave me the chance to procrastinate and discuss general topics ranging from physics to everything else. Therefore a big thank you to Lil' Alex Belin, Elisa Ferreira, Philippe Giguere, Ediot Hijano Cubelos, Guillaume Laporte, Arny Lepage-Jutier, Yuuki Omori, GSalton, Sam Selmani and Kuhan Wang. A special thanks to Arny for the help with the thesis format.

Last and not least, I thank my parents for continuous support throughout my studies even if I choose a path that was unusual to them.

Originality and Contribution of Authors

The original contribution of this work was done under the supervision of Robert Brandenberger. The introduction and chapter 5 of this thesis is based on the preprint *Note on Structure Formation from Cosmic String Wakes* by F. Duplessis and R. Brandenberger [1]. The new distinct contributions to knoweldge were the computation of mass functions for dark matter halos created by cosmic strings wakes. These are found in 5 and allowed us to compare with the predictions of the standard paradigm. Chapter 6 analyses the implications of this result in more details.

1 Introduction

Cosmic strings are linear topological defects predicted by many models of particle physics that go beyond the Standard Model, e.g. in supergravity [2], brane inflation [3] and "String Gas Cosmology" [4] models. In models which admit these defects, a network of cosmic strings is inevitably [5] formed during a phase transition in the very early universe and will persist to the present time. This is true as long as the phase transition occurred after the period of inflation (provided there was inflation). Since strings carry energy, they lead to gravitational effects which induce distinctive signatures in cosmological observations. Since the string tension (which equals the mass per unit length μ) increases as the energy scale η at the time of string formation, the magnitude of the predicted signatures of strings increases as the energy scale grows. Thus, a search for observational signatures of strings allows us to constrain the physics occurring at energies much larger that can be probed by earth-based particle accelerators.

It has long been known that cosmic strings are able to produce many interesting effects for cosmology. In particular, cosmic strings lead to a scale-invariant spectrum of cosmological perturbations [6]. Initially, the focus of interest was on strings which have large enough tension to explain the entire amplitude of the power spectrum [6]. Such strings would need to have a value of the tension given (in dimensionless units) by $G\mu \sim 10^{-6}$, where G is Newton's gravitational constant. The perturbations produced by cosmic strings are, however, active and incoherent [7] and hence do not lead to acoustic oscillations in the angular power spectrum of cosmic microwave (CMB) anisotropies. Thus, when conclusive evidence for the existence of these

oscillations was reached [8], it became clear that cosmic strings could not be the dominant source of structure formation [70] and interest in cosmological effects of strings collapsed. However, in light of the fact that in many models of inflation (or other explanations for the dominant Gaussian component of the power spectrum of cosmological perturbations) cosmic strings are predicted, there has lately been a revival of interest in searching for cosmic strings (see e.g. [10] for a recent survey). A second reason for the revival of interest in searching for strings is that there have been great advances and technological breakthroughs in observational cosmology which are now making it possible to search for signals of cosmic strings with much lower tensions than those previously considered.

The searches have been progressing in many directions. First of all, cosmic strings will contribute to the power spectrum of density fluctuations [6] and to associated CMB anisotropies [11]. Signatures of these fluctuations can be searched for in optical and infrared galaxy surveys and in CMB temperature anisotropy maps. Cosmic strings leave behind distinctive signals in 21cm redshift surveys [82] and in CMB polarization maps [13]. Considerable work has been done to study the effects of strings in the angular power spectrum of CMB temperature and polarization maps [14]. Analyses combining the SPT [15] and WMAP 7-year [16] data were able to place the bound $G\mu \leq 1.7 \times 10^{-7}$ [17] [1], and a similar bound can be obtained [19] using data from the ACT telescope [20]. Improved bounds might be achievable by analyzing CMB maps using statistical tools which are designed to pick out the string-induced non-Gaussianities (see e.g. [21, 22] for some recent studies).

In addition to these purely gravitational effects, cosmic strings can be responsible for the production of highly energetic bursts of particles [23], electromagnetic radiation in a wide range of frequencies [24] and they can help seed coherent magnetic fields on galactic scales [25]. Cosmic string loops decay by emitting gravitational radiation [26]. Hence, strings lead to a scale-invariant stochastic background of

[1] See [18] for earlier bounds using only the WMAP data.

gravitational waves [27] which can be constrained by pulsar timing measurements. Cusps on string loops may lead to additional emission of gravitational waves [28], and a resulting constraint on the cosmic string tension of $G\mu \leq 4\times10^{-9}$ [29] has been reported. However the bound is sensitive to details of cosmic string cusps which are subject to potentially large back-reaction effects [30]. A bound of $G\mu \leq 5.2 \times 10^{-7}$ resulting from constraints on the amplitude of gravitational radiation from pulsar timing constraints is more realistic [31].

Observational optical astronomy is also experiencing a phase of rapid progress. Larger telescopes are probing the universe at increasing depth, i.e. at increasing redshift. Since cosmic strings produce non-linear density perturbations at arbitrarily large redshifts, it is expected that the signals of cosmic strings will stand out from the structures produced by the main source of fluctuations (Gaussian fluctuations) more clearly at high redshifts than at low ones. Signals from structures seeded by string loops has been studied in a recent paper by Schlaer et al. [32] (see also [33] for earlier work) who found that loops could cause significant star formation to occur at high redshift. Therefore cosmic strings with enough mass will have an impact on the epoch of reionization [34, 59]. String loops would also seed dense dark matter clumps whose population today could produce a background of gamma radiation sensitive to the Fermi telescope [36].

In this thesis we address the question of whether cosmic string wakes can produce structures that would allow for observational signatures. In chapter 2 we give a review of the standard knowledge of structure formation. Afterwards we do the same with topological defects in chapter 3, here we mostly focus on covering the notion of cosmic strings along with their dynamics and effects in a cosmological setting. In chapter 4 and 5 we review the literature describing how cosmic strings seeds the growth of structures at very early time. In chapter 5 we also expand on the current literature by computing the mass functions of halos formed in cosmic string wakes and compare them with the expectations from the standard paradigm.

Finally in chapter 6 we explore some observational signals but argue that their detection would be incredibly difficult and also unlikely for the cases we considered.

2

Structure Formation

2.1 Lightning Introduction to Big Bang Cosmology

The big bang picture of the universe is based on the cosmological principle which states that the universe is spatially homogeneous and isotropic on very large scales. A description of the universe that includes these features can be obtained from general relativity by considering the most general metric compatible with the features. This yields the Friedmann-Lematre-Robertson-Walker (FLRW) metric,

$$ds^2 = dt^2 - a(t)^2 d\mathbf{x}^2 = dt^2 - a(t)^2 \Big[\frac{dx^2}{1-kx^2} + x^2 d\Omega^2 \Big]. \tag{2.1}$$

with $d\Omega^2 = d\theta^2 + \sin^2\theta d\phi^2$, and the value $k \in \{0, 1, -1\}$ representing the curvature of the universe. We will assume the universe flat ($k = 0$) in this thesis, we shall soon see how this is justified. The quantity a is called the scale factor and sets the distance between objects on a constant t hypersurface at fixed comoving positions.

Approximating matter by a perfect fluid, spatial homogeneity and isotropy restricts the stress-energy tensor to be of the form,

$$T^{\mu}_{\nu} = diag(\rho, -p, -p, -p). \tag{2.2}$$

The conservation of the stress-energy tensor is written as $\nabla_\mu T^{\mu\nu} = 0$ and its $\nu = 0$ component yields, using the above metric and stress-energy tensor, the continuity equation:

$$\dot{\rho} + 3\Big(\frac{\dot{a}}{a}\Big)(\rho + p) = 0. \tag{2.3}$$

The dynamics of the metric is related to the energy and matter density through the Einstein's equation $G_{\mu\nu} = \frac{1}{M_p^2} T_{\mu\nu}$ where $M_p^2 = (8\pi G)^{-1}$ is the reduced Planck mass. The 00 component and the trace of this equation gives, respectively, the two following Friedmann equations:

$$\left(\frac{\dot{a}}{a}\right)^2 = \frac{1}{3M_p^2}\rho \tag{2.4}$$

$$\left(\frac{\ddot{a}}{a}\right) = -\frac{1}{6M_p^2}(\rho + 3p). \tag{2.5}$$

Solving the Friedmann equation will allow us to obtain the explicit form of $a(t)$. To do so we first need to specify an equation of state (E.O.S.) for matter which we take to be of the form $w\rho = p$ with w constant. Different values of w will describe the evolution of $a(t)$ in a universe dominated by different types of matter. For example, $w = 1/3$ corresponds to a radiation (r) dominated universe, $w = 0$ corresponds to a non-relativistic matter (m) dominated universe and $w = -1$ is from a vacuum energy (Λ) dominated universe. Note that relativistic matter is labelled as radiation since it has $w = 1/3$, when we speak of "matter" we shall refer to the kind that is non-relativistic and hence pressureless $(w = 0)$. Combining the E.O.S. with equations 2.3 and 2.4 we obtain,

$$a(t) \propto t^{1/2} \quad \text{for radiation } (r)$$

$$a(t) \propto t^{2/3} \quad \text{for matter } (m)$$

$$a(t) \propto e^{Ht} \quad \text{for vacuum/dark energy } (\Lambda) \tag{2.6}$$

We define the Hubble parameter $H = \frac{\dot{a}}{a}$. This sets the characteristic (Hubble) time and (Hubble) radius of the universe by $1/H$ (note that we set $c = 1$). We can rewrite the Friedmann equation 2.4 by defining $\rho_c(t) = 3M_p^2 H(t)^2$ and $\Omega_i = \rho_i/\rho_c$ to get,

$$\frac{H(t)}{H_0} = \left[\frac{\Omega_m}{a^3} + \Omega_\Lambda + \frac{\Omega_r}{a^4} + \frac{\Omega_k}{a^2}\right]^{1/2} \tag{2.7}$$

where $H_0 \approx 70.0 \pm 2.2\text{km} \cdot \text{s}^{-1} \cdot \text{Mpc}^{-1}$, $\Omega_m = \Omega_b + \Omega_{dm}$, $\Omega_{dm} \approx 0.233 \pm 0.023$, $\Omega_b = 0.0463 \pm 0.0024$, $\Omega_\Lambda = 0.721 \pm 0.025$, $\Omega_k \approx 0$ [42] are the measured present day value of each quantity after choosing the normalization scale $a(t_0) = 1$. This form makes it easy to see which matter type dominates at which time. For instance, since a increases, our universe will eventually be dominated by the non zero Ω_Λ. The energy of the spatial curvature Ω_k is consistent with zero. Such a small value for this quantity can be explained by inflation and is the reason we have set $k = 0$ in equation 2.1.

There are three important regions of time for which the dynamics of a differs (as shown in 2.6) and hence affects structure formation differently. To determine these we will talk in terms of redshift, which is a very convenient way to parametrize time. A photon's wavelength will get stretched, i.e. redshifted, by the expansion of the universe. By measuring this stretching we can determine how long ago, and also how far away, it was emitted. Let t_0 be the current age of the universe, the redshift is defined as,

$$1 + z(t) = \frac{a(t_0)}{a(t)} = \frac{1}{a(t)}, \tag{2.8}$$

where in the second equality we have used that $a(t_0) = 1$. In the early universe, radiation was the dominant player until matter had time to catch up. The transition from a radiation to matter dominated universe happened at a redshift of $z_{eq} \approx 3300$, the redshift of matter-radiation energy density equality. Afterwards matter dominates until redshift $z < 1$ where the dark energy contribution becomes important.

2.2 Linear Evolution of Newtonian Perturbations

Even though the universe is homogeneous on large scales, it is clear that this does not hold for small scales. The center of the sun looks very different than the near vacuum of outer space. Structures such as galaxies and stars have been created from initially small fluctuations in the energy density, which can be detected as

anisotropies in the CMB's temperature as fluctuations with amplitude of 10^{-5} compared to the background. Here we give a qualitative description of the evolution of density perturbations on small scales (i.e. much smaller than the Hubble radius). We will also assume that the matter and radiation fluid are decoupled. This is the case for the dark matter component at any moment of the universe other than its very beginning.

Since non-relativistic matter in the universe acts like a fluid we can treat the dynamics of perturbations using hydrodynamics, the relativistic case is more complicated and will be ignored here[1]. We will work in comoving coordinates $\vec{x}$ instead of the physical coordinate $\vec{r}$ that we would measure from experiments, they are related by $\vec{r} = a(t)\vec{x}$.

Lets define the pressure by p, the energy density by ρ, the speed of the fluid by $\vec{v}$ and the gravitational potential by Φ and consider the following equations,

$$\begin{aligned} \dot{\rho}_m + a^{-1}\vec{\nabla}_x \cdot (\rho_m \vec{v}) &= 0 \\ \frac{d\vec{v}}{dt} + a^{-1}(\vec{v}\cdot\vec{\nabla}_x)\vec{v} + \frac{1}{\rho_m}a^{-1}\vec{\nabla}_x p_m + a^{-1}\vec{\nabla}_x\Phi &= 0 \\ \nabla_x^2\Phi &= 4\pi a^2 G\rho_t \\ p_m &= p(\rho_m). \end{aligned} \tag{2.9}$$

In order, these equations are: the continuity equation for energy density, the Euler equation, the Poisson equation of Newtonian gravity, and the equation of state. Note how the Poisson equation depends on the total energy density $\rho_t = \rho_m + \rho_r$. The other equations only refer to the matter quantities since it is this part of the fluid that we want to describe. The appearance of ρ_r in the Poisson equation describes how perturbations in the radiation component can seed perturbations in the matter component.

Inserting the following perturbed quantities,

$$\rho_m(t,\vec{x}) = \rho_0^m(t)(1+\delta_m(t,\vec{x}))$$

[1]See [39] or [43] for a relativistic treatment.

$$\vec{v}_m(t,\vec{x}) = \vec{v}_0^m(t,\vec{x}) + \delta\vec{v}_m(t,\vec{x})$$
$$p_m(t,\vec{x}) = p_0^m(t) + \delta p_m(t,\vec{x}). \tag{2.10}$$

in the above ansatz and linearizing to first order, allows us to write the following equation of motion for δ_m, in Fourier space ($\nabla \to \pm ik$),

$$\ddot{\delta_m} + 2H\dot{\delta_m} + c_s^2 k^2 \delta_m - 4\pi G(\rho_0^m \delta_m + \rho_0^r \delta_r) = 0, \tag{2.11}$$

where $c_s^2 = \frac{dp}{d\rho_m}$. This equation describe the dynamics of the matter perturbations δ_m.

In the radiation era, ρ_0^r is dominant so that $H = \frac{1}{2t}$ and any radiation perturbations will seed matter perturbations. Restricting ourselves to the large scale behavior (i.e. $c_s^2 k^2$ is negligible, which is easily attainable for non-relativistic matter where c_s^2 is already quite small), one can show that $\delta_r \propto a(t)^2$ [39]. Using this with the assumption $\rho_0^m \delta_m \ll \rho_0^r \delta_r$, we can find a growing solution of the form $\delta_m \sim \ln(a)$ to equation 2.11. We will see shortly that these perturbations grow much faster in the matter dominated phase.

However we will be mainly interested in the evolution of fluctuation due to cosmic strings which act like a non relativistic matter perturbation such that $\rho_0^m \delta_m \gg \rho_0^r \delta_r$ and hence eq. 2.11 becomes,

$$\ddot{\delta}_m + 2H\dot{\delta}_m = 4\pi G \rho_m \delta_m. \tag{2.12}$$

Since $H^2 = 8\pi G(\rho_m + \rho_r)$ we can define $y = \rho_m/\rho_r$ and rewrite equation 2.12 as,

$$\frac{\partial^2 \delta_m}{\partial y^2} + \frac{2+3y}{2y(1+y)}\frac{\partial \delta_m}{\partial y} - \frac{3}{2y(1+y)}\delta_m = 0. \tag{2.13}$$

This has two solutions, namely [40]

$$D_1(y) = y + 2/3, \tag{2.14}$$

$$D_2(y) = D_1(y)\ln\Big[\frac{\sqrt{1+y}+1}{\sqrt{1+y}-1}\Big] - 2\sqrt{1+y}. \tag{2.15}$$

Hence in the radiation dominated era where $y \ll 1$ the perturbation does not grow appreciably. Moreover since the radiation growth is independent on the CDM perturbations to zero'th order in y then, to linear order, cosmic strings will seed no growth of matter perturbations before t_{eq}, which is the time when our universe becomes matter dominated! This growth impediment of matter perturbations in the radiation era is called the *Meszaros effect*.

In the matter dominated regime, the Hubble constant is now $H = \frac{2}{3t}$ and radiation perturbations are negligible so that equation 2.11 becomes,

$$\ddot{\delta_m} + \frac{4}{3t}\dot{\delta_m} + (c_s^2 k^2 - 4\pi G \rho_0^m)\delta_m = 0, \tag{2.16}$$

Equation 2.16 introduces a length scale, called the Jeans length, defined by the wavelength with wavevector $k_J = \left(\frac{4\pi G \rho_0^m}{c_s^2}\right)^{1/2}$. This length scale marks the transition between when the outward fluid pressure or the inward gravitational force becomes the dominant effect. For $k \gg k_J$ the pressure dominates and perturbations have a decaying oscillatory solution,

$$\delta_k(t) \sim a^{-1/2} \exp\Big[\pm i c_s k \int dt' a(t') \Big], \tag{2.17}$$

while for $k \ll k_J$ matter is accreted by gravitational infall and we obtain,

$$\delta_k(t) = c_1 t^{2/3} + c_2 t^{-1/2}. \tag{2.18}$$

Hence one solution is growing as the scale factor $a(t)$ and the other is decaying. If we use a more general H which also incorporates the effect of a non zero cosmological constant Λ, we find that the growing mode can be given by a growth factor $\delta_m \sim D(t)$ [41] where,

$$D(t) \propto \frac{(\Omega_\Lambda a^3 + \Omega_m)^{1/2}}{a^{3/2}} \int_a \frac{a^{3/2} da}{(\Omega_\Lambda a^3 + \Omega_m)^{3/2}}. \tag{2.19}$$

Note that the effect of Hubble friction (the $3H\dot{\delta}_m$ term in 2.16) is drastic to the dynamics of perturbations: if $H = 0$ the solution of modes with $k < k_J$ would grow exponentially.

2.3 Non-linear growth

To study the evolution of matter overdensities in the non-linear regime, we use the simplified assumption that we are dealing with a localised spherical overdensity. We also assume that we are in an Einstein-de Sitter universe ($\Omega_m = 1,\ \Omega_r = \Omega_\Lambda = 0$), which is a valid approximation for $1 \leq z \leq z_{eq}$.

Following the discussion in section 8 of Padmanabhan's book [43], we consider a sphere of radius r centered around the spherical perturbation. We write the energy density inside the shell as $\rho = \rho_0 + \delta\rho = \rho_0(1+\delta)$ and follow the trajectory of a particle at the boundary which obey the as equation of motion (EOM),

$$\ddot{r} = -\frac{GM_0}{r^2} - \frac{G\delta M}{r^2}, \tag{2.20}$$

where $M_0 = \frac{4\pi}{3}\rho_0 r^3 = \text{constant}$ and $\delta M = \int_V \mathrm{d}^3x\delta\rho$ with V being the shell's volume. We can write $\ddot{r} = -\frac{GM}{r^2}$ with $M = \rho_0(t_i)\frac{4\pi}{3}r_i^3(1+\bar{\delta}_i)$ where the subscript i denotes that we are dealing with the initial value of each quantity and the bar denotes the average inside the shell. A shell will be bound and eventually turn around if its energy is smaller than 0: $E = K_i + U_i < 0$. The initial kinetic energy of the particles on the shell comes from the Hubble flow $K_i = \frac{H_i^2 r_i^2}{2}$ while the gravitational energy is $U_i = \frac{GM}{r_i} = \frac{1}{2}H_i^2 r_i^2(1+\bar{\delta}_i)$. Since at turnaround all the energy is in U, we can find the radius at which this happens. By equating

$$E_i = \frac{GM}{r_{ta}} = U(t_{ta}),$$

then given a surface with initial radius r_i we find the turnaround radius r_{ta} to be,

$$\frac{r_{ta}}{r_i} = \frac{(1+\bar{\delta}_i)}{\bar{\delta}_i}. \tag{2.21}$$

We can also write the solution to equation 2.20 in parametric form by using

$$r = A(1-\cos(\theta)), \quad A = \frac{r_{ta}}{2} = \frac{r_i}{2}\frac{1+\bar{\delta}_i}{\bar{\delta}_i} \tag{2.22}$$

$$t + T = B(\theta - \sin(\theta)), \quad B = \left(\frac{A^3}{GM}\right)^{1/2} = \frac{1+\bar{\delta}_i}{2H_i\bar{\delta}_i^{3/2}}. \tag{2.23}$$

At t_i we must impose the boundary conditions $r(\theta_i) = r_i$ and $t(\theta_i) + T = t_i + T$ which allows us to determine T and θ_i. The turnaround angle is $\theta = \pi$ so given $\bar{\delta}_i$ and r_i we can write down the turnaround time,

$$t_{ta} = \frac{1}{2H_i}\Big(\frac{1+\bar{\delta}_i}{\bar{\delta}_i^{3/2}}\Big)(\pi - \theta_i + \sin(\theta_i)) + t_i, \tag{2.24}$$

with $\theta_i = \mathrm{ArcCos}\big(1 - \frac{2\bar{\delta}_i}{1+\bar{\delta}_i}\big)$. More importantly, we can also give an expression for the average density within our shell $\rho(t) = \frac{3M}{4\pi r^3}$ by replacing $\{M,\ r\}$ by $\{t,\ \theta\}$,

$$\frac{\rho(\theta,t)}{\rho_0(t)} = \frac{9}{2}\frac{(\theta - \sin\theta)^2}{(1-\cos\theta)^3}, \tag{2.25}$$

here $\rho_0 = 1/(4\pi G t^2)$ is the background density of the universe. At turnaround we find $\rho/\rho_0 \approx 5.6$ which means that **any** spherical shell that collapses does so when it becomes 5.6 times denser than the background. In other words, the concentric shells slows down at different rate (faster for smaller ones) and hence their density decreases at a smaller rate than the background.

At some point the shells decouple from the Hubble flow and start collapsing. This increases the density inside the shell until the pressure and gravitational force finds an equilibrium state. According to the virial theorem, this balance happens when $2K = -U$ and implies a virialized radius that is half of the turnaround radius $2r_{vir} = r_{ta}$, hence the density increases by a factor of 2^3 from the value at turnaround. By symmetry it should also take as long for the shell to collapse as it took it to decouple from the Hubble flow, hence $t_{col} = 2t_{ta}$ and so the background density has time to decay by a factor of 2^2. Therefore we consider objects that has $\rho(t)/\rho_0(t) \approx 2^2 \times 2^3 \times 5.6 \approx 180$ to be virialized. This allows us to determine the properties of our defined collapsed objects such as their radius r_{vir}, simply from by knowing their mass M and the redshift z at which they collapsed [41],

$$M \approx \frac{4\pi}{3} r_{vir}^3 180 \rho_0(z) \rightarrow r_{vir} \approx \Big(\frac{GM}{90H_0^2}\Big)^{1/3}\frac{1}{1+z}. \tag{2.26}$$

Using this and the virial theorem, we are able to find the average kinetic energy of the halo's protons and hence its temperature. Let m_p be the protons mass and k_b the Boltzmann constant,

$$T_{vir} = \frac{m_p v_{vir}^2}{3k_b} = \frac{m_p}{3k_b}\Big(\frac{GM}{r_{vir}}\Big) \approx 1.5\frac{m_p}{k_b}(H_0 GM)^{2/3}(1+z). \tag{2.27}$$

This temperature holds valuable information. If it is high enough so that the hydrogen atoms have enough energy to excite each other in inelastic collisions, then as they bump into each other, they radiate away as they transition back to their ground state. Hence the overall kinetic energy in the hydrogen atoms drops and the gas condenses towards the center of the halo. This is how the density of matter is able to increase in order to eventually give rise to stars. The required temperature to have efficient star formation is usually taken to be 10^4 degree kelvins. We will discuss this in more detail when determining if structures created by strings can harbor star formation. Note that the picture is different for dark matter since it has very weak interactions; dark matter particles cannot lose their kinetic energy through collisions and therefore their distribution stays very spread out. This is why we refer to dark matter *halos* around galaxies and their clusters. We will employ this terminology to talk about collapsed clumps of matter.

2.4 Predicting the number of virialized objects

We now turn our attention to the Press-Schechter formalism which gives an estimate of the number of halos with a given mass at different redshifts. Our previous exploration of the non-linear regime is useful in that it allows us to talk about non-linear dynamics using linear perturbation theory. In the linear regime we have $\delta_L(t) = \bar{\delta}(t_i)D(t)/D(t_i)$. Inserting the time of virialization ($2t_a$) into this ansatz we obtain $\delta_L = 1.686$ for an Einstein-de Sitter universe [41]. The linear analysis underpredicts the actual value by a factor of 100, but this is fine if we are just interested in devising a condition that tells us **when** stuff has collapsed. Our condition is simply

that regions of space have virialized at the time their linear overdensity has grown to a value $\delta_L = 1.686$!

We will see how this is useful in a moment. We wish to predict the number of collapsed objects of different mass that we should observe. Performing such a prediction requires us to determine the value of $\bar{\delta}(t_i, R)$, the initial average overdensity on a comoving length scale R. This will be a statistical value given by the root mean square in the initial density fluctuation. Consider the Fourier modes $\delta_{\mathbf{k}}$ of the local overdensity $\delta(\mathbf{x})$ which are given by,

$$\delta_{\mathbf{k}} = \int dx^3 \delta(\mathbf{x}) e^{-i\mathbf{k}\cdot\mathbf{x}}. \tag{2.28}$$

Far in the past, the value of each mode $\delta_{\mathbf{k}}$ is drawn from a nearly Gaussian distribution. This statement can be made since $\delta(x)$ at the time of recombination t_{rec} is related to the CMB anisotropies: photons trying to escape dense regions gets redshifted by escaping their gravitational well and hence the temperature in that location decreases. These CMB anisotropies can be measured and the modes in their Fourier decomposition have this Gaussian property, hence so must $\delta_{\mathbf{k}}$. We can characterize the variance of $\delta_{\mathbf{k}}$ by the power spectrum $P(k)$ defined by,

$$\langle \delta_{\mathbf{k}} \delta^*_{\mathbf{k}'} \rangle = (2\pi)^3 P(k) \delta^{(3)}(\mathbf{k} - \mathbf{k}'). \tag{2.29}$$

Inflationary scenarios predict that $P(k) \propto k^n$ with $n \approx 1$, this is called a scale invariant spectrum. However as the modes enter the horizon recall that they start to evolve in different ways depending on whether we are in the radiation or matter dominated era. This leads to a turnover in the power spectrum at the scale of equal matter-radiation energy density k_{eq}^{-1}. Therefore on scales $k \ll k_{eq}$ we have $P(k) \propto k$ while for $k \gg k_{eq}$ we have $P(k) \propto k^{n-4}$. Figure 2.1 shows the current large scale power spectrum. Note the bend at $k_{eq} \approx 0.01\ h/Mpc$ and the subsequent oscillations, here we introduced $h = \frac{H_0}{100} \frac{\text{s Mpc}}{\text{km}} \approx 0.7$.

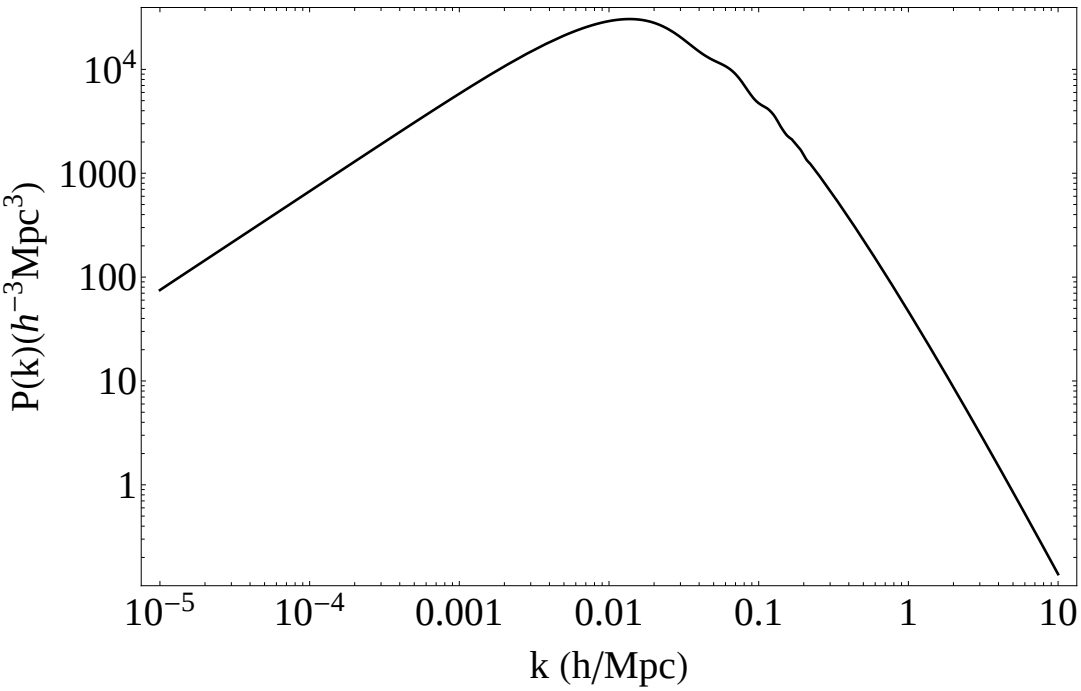

Figure 2.1: Current day power spectrum on large scales which are still well approximated by linear perturbation theory. On smaller scales, gravitational clustering becomes important and corrections to the linear theory must be considered. This can be done analytically by adding loop corrections to our original two point function [45] or, as studied more recently, by taking an effective field theory approach [46]. However to obtain the power spectrum on very non-linear scale we must resort to N-body simulations. This power spectrum was plotted using data supplied by [47]

One can use the power spectrum to determine the variance of mass fluctuation on a given comoving length scale R. Consider a sphere of comoving radius R, we define the window function $W(\mathbf{y})$ to equal $3/(4\pi R^3)$ inside the sphere and 0 outside so that $\int dy^3 W(\mathbf{y}) = 1$. We can then construct the smoothed density perturbation field $\delta_W(\mathbf{x}) = \int dy^3 \delta(\mathbf{x}+\mathbf{y})W(\mathbf{y})$ which follows a Gaussian distribution of zero mean. The variance of the overdensity inside the sphere $\langle \delta_W(\mathbf{x})^2 \rangle = \sigma^2(R)$ can then be expressed in the nice form,

$$\sigma^2(R) = \int_0^\infty \frac{dk}{2\pi^2} k^2 P(k) \Big[\frac{3j_1(kR)}{kR}\Big]^2, \tag{2.30}$$

where $j_1(kR) = \big(\sin(kR) - kR\cos(kR)\big)/(kR)^2$ is a factor coming from the Fourier transform due to $W(x)$. The theory does not allow us to calculate the overall normalisation of the power spectrum, therefore it is customary to normalise it so that it agrees with the measured value of $\sigma_8 = \sigma(R = 8h^{-1}\text{Mpc})$. According to the WMAP 9-year results [42], $\sigma_8 = 0.821 \pm 0.023$.

Now lets see how to use $\sigma(R)$ to estimate the number of dark matter halos. The power spectrum is redshift dependent but we can evolve it linearly to the present day, this yields a linear value of $\sigma(R)$ at some fixed redshift which we take to be 0. One might ask the question: what is the probability that a sphere of comoving radius R has an average linear overdensity larger than δ' at $z = 0$. Since $\sigma(R)$ measures the variance of such fluctuations, the answer will simply be

$$P(>\delta') = \int_{\delta'}^\infty \frac{1}{\sqrt{2\pi\sigma(R)^2}} \exp(-\tilde{\delta}^2/(2\sigma(R)^2)) d\tilde{\delta}. \tag{2.31}$$

Now recall that a region with $\delta' = 1.686$ implies that the mass contained inside it must have collapsed into a virialized object. Now define,

$$\delta_c(z) = \frac{1.686}{D(z)}, \tag{2.32}$$

where $D(z)$ is the growth function, as defined in 2.19, and normalized such that $D(0) = 1$. Then for $\delta' = \delta_c(0)$ the quantity in equation 2.31 measures the probability

that a region of comoving radius R has collapsed at $z = 0$ and is now part of a halo! We can do this for any z. A region that has collapsed at redshift z will have $\delta_{lin}(z) \geq 1.686$ at that redshift, so this implies a $\delta_{lin}(0) = \delta' \geq \delta_c(z)$ after linearly interpolating to redshift 0 and using this value in 2.31 would give us the probability that such a region collapsed at a redshift z. An apparent problem here is that the quantity 2.31 is always smaller than 1/2. To fix this we must multiply the final answer by 2. Therefore the probability that the mass inside a comoving sphere of radius R has collapsed at redshift z is given by,

$$P(R, z) = 2 \int_{\delta_c(z)}^{\infty} \frac{1}{\sqrt{2\pi\sigma(R)^2}} \exp(-\tilde{\delta}^2/(2\sigma(R)^2)) d\tilde{\delta}. \tag{2.33}$$

$$= \text{Erfc}\Big(\frac{\delta_c(z)}{\sqrt{2}\sigma(R)}\Big). \tag{2.34}$$

The seemingly ad hoc factor of 2 takes into account regions that have $\delta' < 1.686$ but might be part of larger regions who themselves have $\delta' \geq 1.686$. It was shown by Bond et al. [44] that those situations gave precisely this extra factor of 2.

As we've seen in the previous section, we can write a relation between a comoving volume R and the mass it contains at a given redshift by considering the background density $\rho(z)$,

$$M = \frac{4\pi}{3} R^3 \rho(z). \tag{2.35}$$

Hence instead of speaking of the probability that the mass in a comoving volume V has collapsed, we can speak of the probability that a halo of mass M has formed. The probability in equation 2.33 can also be interpreted as the fraction of matter in bound halos. At a given redshift $\mathrm{d}P = P(M) - P(M - \mathrm{d}M)$ would count the fraction of particles in halo's of mass $[M - \mathrm{d}M, M]$, this allows us to finally write an expression for the **comoving number density of halos** of mass M,

$$n(M)\mathrm{d}M = \frac{\rho}{M} \frac{\mathrm{d}P}{\mathrm{d}M} \mathrm{d}M, \tag{2.36}$$

and the **comoving mass function** which describes the amount of matter found in halos of a given mass,

$$\frac{\mathrm{d}n}{\mathrm{d}(\ln\, M)} = -\sqrt{\frac{2}{\pi}}\rho\frac{\mathrm{d}(\ln\, \sigma(M))}{\mathrm{d}M}\frac{\delta_c(z)}{\sigma(M)}\exp\Big(\frac{\delta_c(z)^2}{2\sigma(M)^2}\Big). \tag{2.37}$$

This whole treatment to estimate the halo distribution is called the Press-Schechter formalism and the extended Press-Schechter formalism when considering the additional factor of 2. This crude way of estimating the halo distribution might seem to be overlooking many important effects, and it does, but it matches surprisingly well the numerical simulations over a wide range of magnitude. A more modern approach would be to introduce tunable parameters in the expression 2.37 and fit them to N-body simulations. This leads to mass functions giving slightly different results and the Sheth-Tormen [48] mass function is a famous example of this. Figure 2.2 compares these different mass functions using the input parameters from WMAP's measurements and figure 2.3 plots the mass function fitted by Reed et al. [47] at different redshifts.

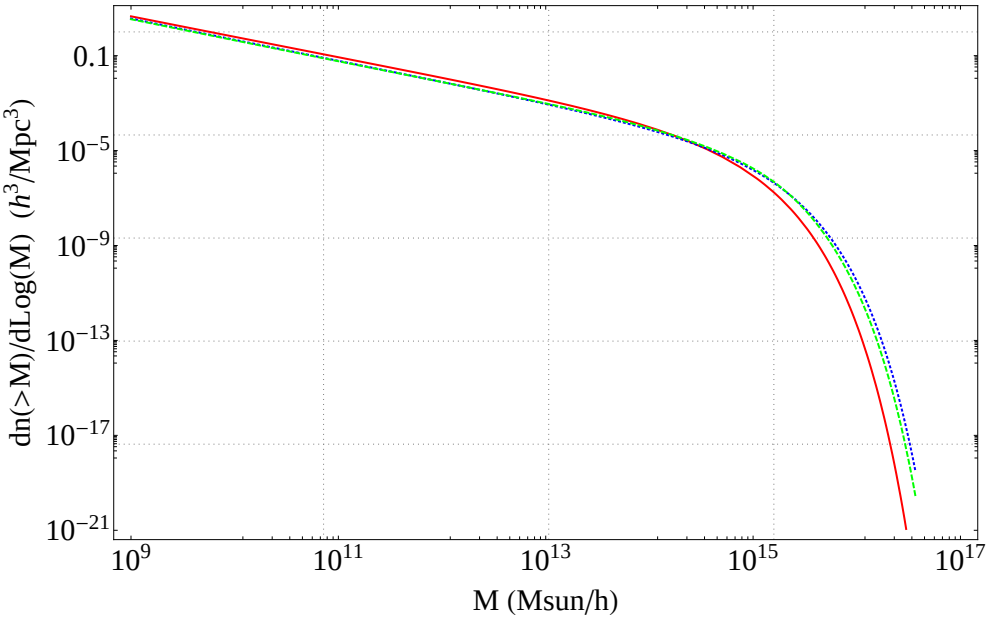

Figure 2.2: Comoving Mass function of DM halos. The red solid one is using the original Press-Schechter formalism while the blue dotted and green dashed ones are the Sheth-Tormen (1999) [48] and Reed et al. (2006) [47] predictions respectively.

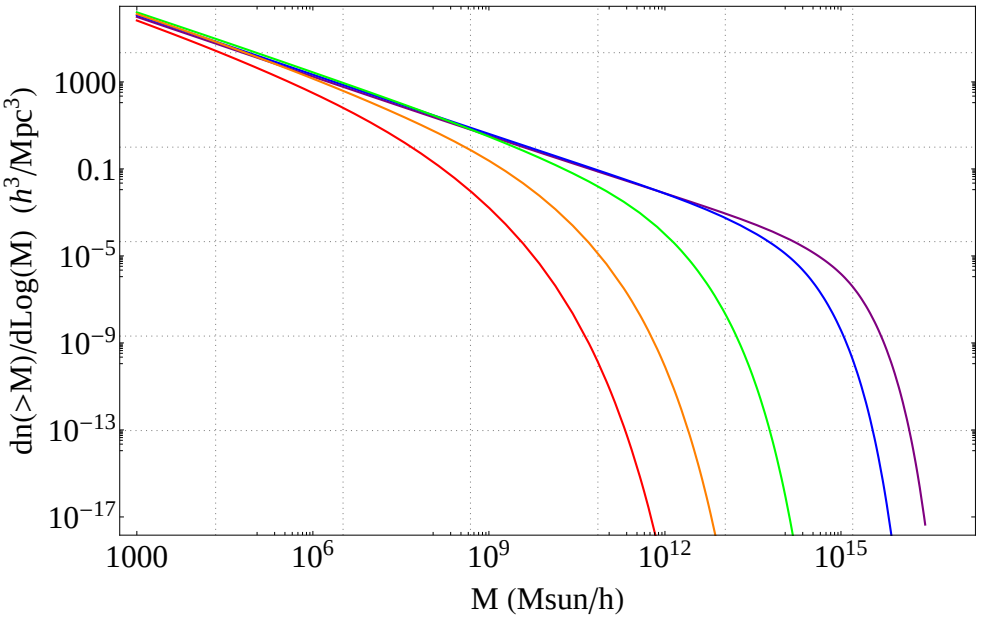

Figure 2.3: Reed et al. comoving Mass function of DM halos at redshifts 0 (purple), 1 (blue), 5 (green), 10 (orange), 15 (red). Note how the mass functions take on lower values at lower redshifts on small scales.

3

What are Cosmic Strings?

Inflation is not the only mechanism that can produce inhomogeneities which give rise to the structures we see in the universe. As mentioned in the introduction, cosmic strings is one such mechanism and we wish to determine if they could produce observable signals in the large scale structure. In order to explore this possibility we now give an introduction to the notion of topological defects, in particular cosmic strings.

Certain field theories allow for static field configurations that are distinct from the vacuum solution and are stable due to topological reasons. These configurations, called **topological defects**, possesses regions where the energy density is non-zero. One can imagine how these can have cosmological implications since they are a generic property of many particle physics models and hence are expected to be produced in the very early universe. Cosmic defects have yet to be observed, but their stability assures that they should still be here today if they were produced after the inflationary epoch. Actually one of the original motivations for inflation [49] was to dilute the enormous amount of gauge monopoles: these are spherical defects predicted by grand unified models and would be produced in such a large quantity that it would strongly disagree with observations [50]. Topological defects are still not seen in the sky but they are quite common in condensed matter physics, some examples are: two dimensional **domain walls** are found in ferromagnet at the

boundary between regions with different magnetic dipoles alignment, one and zero dimensional defects such as **strings** and **monopoles** respectively can be found in liquid crystals (figure 3.1).

Any construction of defects must be consistent with Derrick's theorem [52] which states that there cannot be localized, time-independent stable solution from scalar theories described by the follow Lagrangian with $D > 1$,

$$\mathcal{L} = \frac{1}{2}\partial_\mu \phi^\dagger \partial^\mu \phi - V(\phi). \tag{3.1}$$

The proof of the theorem goes as follows [53]: suppose we have a localised solution with finite energy

$$E = \int d^D x \Big[\frac{1}{2}(\nabla\phi)^2 + V(\phi)\Big], \tag{3.2}$$

then rescaling $\mathbf{x} \to \alpha\mathbf{x}$, the energy rescales accordingly to,

$$E \to E' = \int d^D x \Big[\frac{1}{2}(\nabla\phi)^2 \alpha^{2-D} + V(\phi)\alpha^{-D}\Big]. \tag{3.3}$$

If $V(\phi) \neq 0$ and $D > 1$, a rescaling of the problem lowers the energy of the configuration and therefore it will be unstable to collapse. We shall consider two extensions of the above model, these will yield stable defects. The first extension drops the requirement of locality, giving rise to **global** defects which allows for long range forces between them. The second extension is to add gauge fields to our Lagrangian which can take a stabilizing configuration, we call those **gauge** defects.

3.1 Topological defects

We will give an overview of the conditions required for the formation of topological defects and give specific example of each type found in 3+1 dimensions using scalar fields. Before doing so we introduce the concept of **homotopy group** of a manifold M.

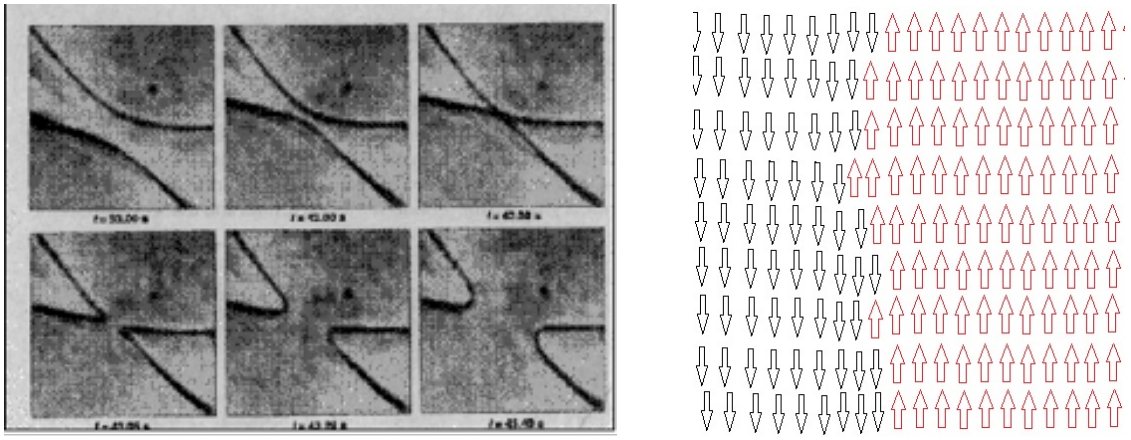

Figure 3.1: Intercommuting strings in a liquid crystal (right) [51]. The boundary between two regions with different spin orientation forms a domain wall in ferromagnet (left).

Definition: The n^{th} homotopy group of a manifold M at x denoted by $\pi_n(M, x)$, is the set of all homotopically distinct maps $f : S^n \to M$ such that there is $a \in S^n$ for which $f(a) = x$.

Essentially, $\pi_n(M, x)$ contains the equivalence class of different maps $f : S^n \to M$ that cannot be continuously deformed (i.e. aren't **homotopic**) into each other; if $f,\ g : S^n \to M$ are homotopic, then $[f] = [g] \in \pi_n(M, x)$. Notice that the requirement that f goes through the basepoint x can be dropped for path connected manifolds since the homotopy groups of M at any two basepoints are isomorphic. Other than in the case of the domain wall, our manifolds of interest will be path connected. Thus, whenever we talk about π_n for $n \geq 1$, we will simply talk about the n^{th} homotopic group of the manifold M denoted $\pi_n(M)$. When M is not connected then $\pi_n(M)$ is not a group. Note that $\pi_0(M)$ is only non-trivial when M is not connected since otherwise we can always bring two points together; the elements of $\pi_0(M)$ labels the disconnected components of M.

This machinery will helps us classify different kinds of defects, so lets jump into our first example to see how it achieves that.

The Domain Wall

Consider a single real scalar field in $1+1$ dimension with Lagrangian density and potential,

$$\mathcal{L} = \frac{\dot{\phi}^2}{2} - \frac{(\partial_x \phi)^2}{2} - V(\phi), \quad V(\phi) = \frac{\lambda}{4}(\phi^2 - \eta^2)^2. \tag{3.4}$$

This has as static solution $\phi(x) = \eta \tanh\left(\sqrt{\frac{\lambda}{2}}\eta x\right)$ and is sketched with the potential in figure 3.2. The solution goes to $\pm\eta$ as $x \to \pm\infty$, hence the energy density vanishes and is finite overall, only departing from zero near where $\phi = 0$. The existence of such a solution is related to our homotopy discussion in the following way. We define the vacuum manifold $\mathcal{M}$ to be the set of field values that minimize the potential energy. In our case $\mathcal{M} = \{\pm\eta\}$ is a disconnected set of two points, so its 0^{th} homotopy group $\pi_0(\mathcal{M})$ is isomorphic to $\mathcal{Z}_2$. Our solution at must therefore interpolate between these two disconnected point that can only achieve that continuously by leaving the vacuum manifold. This feature give rise to a conserved topological charge $N = \int dx \partial_x \phi = 2\eta$ which is carried by **topological** defects and responsible for their stability.

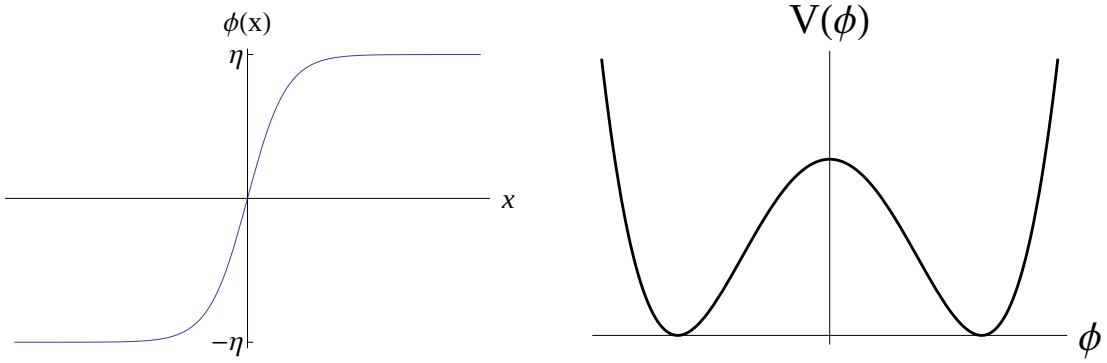

Figure 3.2: Sketch of the soliton solution in one dimension.

In this way, looking at the homotopy groups of the vacuum manifolds allows us to determine the existence of defects in the theory and then we can classify them by their $\pi_n(\mathcal{M})$. Table 3.1 lists the allowed defects in 3+1 dimensions. We look at the possible ways to map a region in physical space, that can have the topology of

Homotopy group	Name of Defect	local	global
$\pi_0(\mathcal{M}) \neq 1$	Domain Wall	X	X
$\pi_1(\mathcal{M}) \neq 1$	Cosmic Strings	O	O
$\pi_2(\mathcal{M}) \neq 1$	Monopoles	X	O
$\pi_3(\mathcal{M}) \neq 1$	Textures	N.A.	O

Table 3.1: Classification of defects in 3+1 dimension and if they are incompatible (X) or compatible (O) with current cosmological observation. This figure was reproduced as found in [10].

$S^0, ..., S^3$, into the vacuum manifold $\mathcal{M}$ which gives us 4 possible defects.

Neglecting Derrick's theorem for a moment, we can easily imagine extending the kink to form a similar solution in 3+1 dimensions by having translational symmetry in y, z to obtain a domain wall. Theories with domain walls are ruled out since they would quickly dominate the energy density of the universe: the energy density per unit surface is given by

$$\sigma_E \sim V(\phi = 0) \times \text{width} \sim \frac{\lambda\eta^4}{\lambda^{1/2}\eta} = \lambda^{1/2}\eta^3, \tag{3.5}$$

which means that with the Hubble expansion - characterized by the scale factor a(t) - the domain wall's surface increases as $A(t) = A_0 a(t)^2$ while σ_E stays constant. For non-relativistic walls, their density is redshifted by a factor of $1/a(t)^3$, hence the total energy density scales as $1/a(t)$. As we discussed in section 2.1, the energy density of matter and radiation scales as a^{-3}, a^{-4} respectively, hence domain walls should quickly dominate the evolution of the universe and this is not observed.
Vacuum manifolds that have non trivial π_1, π_2 and π_3 give rise to cosmic strings, monopole and textures respectively. Note that, naively, applying a similar argument to cosmic strings would imply that they should be ruled out. However a more detailed analysis taking into account string interactions changes this conclusion and will be presented in section 3.3.1.

The Cosmic String

Our cosmic strings will live in $3+1$ dimensions and therefore we must consider the cases that evade Derrick's theorem. We will focus on gauge strings and mention how global strings differ. Consider a complex scalar field ϕ with a $U(1)$ gauge symmetry giving rise to a gauge field A_μ.

$$\mathcal{L} = \frac{1}{2} D_\mu \phi^\dagger D^\mu \phi - V(\phi) + \frac{1}{4} F_{\mu\nu} F^{\mu\nu} \tag{3.6}$$

Here $D_\mu = \partial_\mu + igA_\mu$ and $F_{\mu\nu}$ is the stress energy tensor. We choose the "Mexican hat" potential $V(\phi) = \frac{1}{4}(\phi^\dagger\phi - \eta^2)^2$ (figure 3.3) which has as vacuum manifold $\mathcal{M} = \{e^{i\theta}\eta \ : \ \theta \in [0, 2\pi)\}$. $\mathcal{M}$ possess the same topology as a circle, therefore $\pi_1(\mathcal{M}) = \mathbb{Z}$ and characterizes maps with different winding numbers $n \in \mathbb{Z}$. In the Lorentz gauge $\partial_\mu A^\mu = 0$, a static solution can have the asymptotic form $\phi(r, \theta, z) \approx e^{im\theta}\eta$ for large r with m being an integer. This is a field configuration that winds around the vacuum manifold m times and is independent of z. The solution near $r \approx 0$ must climb up the potential otherwise we could shrink a winding path in physical space until it lies on a single point and this would imply that we have a point with $|\phi| = \eta$ but without a well defined phase. Therefore we define the point (r', θ', z) such that $\phi(r', \theta', z) = 0$ to be the center of the cosmic string. On the other hand, the gauge field takes the asymptotic form $A_\mu \approx \frac{1}{ie}\partial_\mu \ln\phi$, note that it is not exact since $\ln\phi$ is a multivalued function and so we cannot gauge it away. One can compute the flux through a path encircling the string,

$$\Phi_B = \int \mathbf{B} \cdot \mathrm{d}\mathbf{S} = \oint \mathbf{A} \cdot \mathrm{d}\mathbf{l} = \frac{2\pi m}{e}, \tag{3.7}$$

which shows that a gauge cosmic string possesses a magnetic flux flowing through it.

The energy density per unit length is finite for a gauge string since $D_\mu\phi \approx 0$, $F_{\mu\nu} \approx 0$ away from the core. Moreover, the characteristic length scale associated with each field gives us the approximate width of our string, namely it has a core of false vacuum of radius $\delta_\phi \ m_\phi^{-1} = (\sqrt{\lambda}\eta)^{-1}$ where $V(\phi) \sim \lambda\eta^4$, and a flux tube of

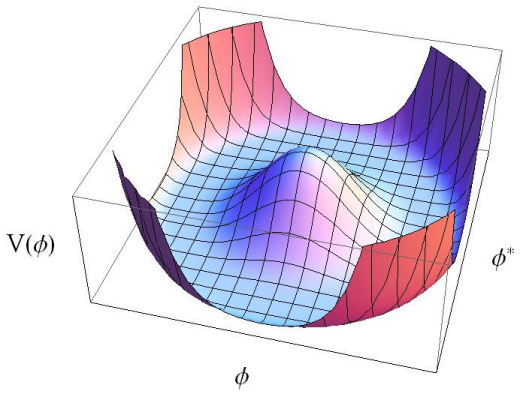

Figure 3.3: Sketch of the Mexican hat potential responsible for cosmic strings.

radius $\delta_A \sim m_A^{-1} = (e\eta)^{-1}$ containing a magnetic field $B \sim \Phi_B/\delta_A^2$. Hence the string tension, which is the energy per unit length, is $\mu \sim \delta_\phi^2 V(\phi) + \delta_A^2 B^2 \sim \eta^2$. This will be a very important quantity and the main parameter that we will try to constrain with observations. Great information about high energy physics is found in μ since, as we will see shortly, η is related to the energy scale at which cosmic strings form.

The global string, although it possess a scalar field configuration of the same form as the gauge string, differs in energy density due to the lack of gauge field that can absorb the gradient energy at large r (i.e. $\partial_\mu \phi \neq 0$ unlike $D_\mu \phi \approx 0$ for gauge string). The tension for such strings goes as

$$\mu \sim \int_\delta^R 2\pi r dr \Big(\frac{1}{r}\frac{\partial \phi}{\partial \theta}\Big) \approx 2\pi\eta^2 \ln\big(\frac{R}{\delta}\big), \tag{3.8}$$

where R is a large cutoff that will be determined by the string's curvature or by the distance to the nearest other string. Both global and gauge string are still consistent with observations and hence allowed to exist in our universe. However we shall focus on the gauge string when discussing gravitational implications. The main reason is that gauge symmetries are favored over global symmetries in particle physics models. Nevertheless it is argued that the cosmological implications are very similar in both cases [53]. For instance, their different tensions will be the only difference in the scaling behavior of their energy density, a topic we will discuss in section 3.3.

Before dwelling into finer details of cosmic strings, we will mention a few words about monopoles and textures.

The Monopole and the Texture

To get a monopole we need a vacuum manifold with non contractible spheres, namely $\pi_2(\mathcal{M}) \neq 0$. A simple example is a field theory with scalars ϕ_a, $a \in \{1, 2, 3\}$ and potential $V = \frac{\lambda}{4}(\sum_a \phi_a^2 - \eta^2)^2$. A solution taking the form of $\vec{\phi} = \eta\hat{\mathbf{r}}$ (where $\hat{\mathbf{r}}$ is the unit radial vector) at large r yields a monopole. As in the string case, we can add a gauge field to our theory which will soak up the gradient energy so that the total energy of our field configuration remains finite. In that situation, the gauge field configuration would produce a magnetic field which would impart a magnetic charge to the monopole. As discussed in the introduction, the formation of gauge monopoles would be a disaster since these don't dilute fast enough and would dominate the energy density. However in the case of global monopoles, long range forces allows them to strongly interact and settle in a scaling solution in such a way that only a few monopoles are present per horizon volume [54]. Therefore no current cosmological constraint allow us to rule them out.

Finally, textures come from some $\mathcal{M}$ with $\pi_3(\mathcal{M}) \neq 0$. Note this implies that a field configuration giving rise to a texture in our universe can lie solely in $\mathcal{M}$ and have only gradient energy. This means that adding a gauge field would simply cancel any effect of the texture. Moreover the fact that the field configuration does not leave the vacuum manifold implies that there is no topological charge associated to textures and thus that they are not stable. If we recall Derrick's theorem, the energy in textures scales as $E \propto \alpha^{-1}$ under $\mathbf{x} \to \alpha\mathbf{x}$, therefore textures shrink and eventually decay.

3.2 How does Cosmic String formation arise from Particle Physics?

Mexican hat potentials generic for many scalar fields in particle physics model. One such example is the Higgs field which give the fermions their masses. These potential have finite temperature corrections which can alter the effective vacuum manifold. To find those corrections we note that quantum fields at finite temperature tend to minimize their free energy F which, assuming the chemical potential is zero, is given by

$$F = E - TS, \tag{3.9}$$

where E is the energy, T is the temperature and S the entropy. At low T this is minimized when $\phi \in \mathcal{M}$ however as T increases the second term become important and higher temperature allows for more states to be accessible. An intuitive picture is that the field's fluctuations become increasingly large with temperature and hence small features of the potential - such as the double well - have no effect on its dynamics.

It was shown (see p.40 of [53]) that the free energy of a QFT can be computed from the same diagrams as the effective potential but with finite temperature Green's function, i.e.

$$F = -\frac{1}{\beta}\log Z(\beta), \tag{3.10}$$

with $Z(\beta)$ being the Euclidean path integral. The free energy per unit volume is called the effective temperature potential, and is given by

$$V_{eff}(\phi, T) = V(\phi) + \sum_n F_n(\phi, T), \tag{3.11}$$

where,

$$F_n = \pm T \int \frac{dk^3}{(2\pi)^3} \ln(1 \pm \exp(\epsilon_k/T)),\ \epsilon_k = (k^2 + m_n^2)$$

Here F_n is the contribution to the free energy of different spin states of the various fields. The fermions come with the $-$ sign while the bosons come with the $+$ sign. At temperatures much lower than the mass scale $m_n \gg T$ we can neglect the F_n, but in the other extreme $T \gg m_n$ we can evaluate the integral to get,

$$F_n = -\frac{\pi^2}{90}T^4 + \frac{m_n^2 T^2}{24} + \mathcal{O}(M_n)^4 \qquad \text{for fermions,} \tag{3.12}$$

$$F_n = -\frac{7\pi^2}{720}T^4 + \frac{m_n^2 T^2}{48} + \mathcal{O}(M_n)^4 \qquad \text{for bosons} \tag{3.13}$$

where the mass of each particle type is given by the Higgs mechanism. Namely if we couple both fields with a term in the Lagrangian such as $\sim \phi^2\psi^2$, then when ϕ takes a non-zero vacuum expectation value (VEV) it produces a mass term $\sim \langle\phi^2\rangle\psi^2 = m_\psi^2\psi^2$. For example, using the potential in equation 3.6 we end up with an effective potential (see [53] for more details on the derivation),

$$V_{eff} = \frac{\lambda}{12}(T^2 - 6\eta^2)\phi^\dagger\phi + \frac{\lambda}{4}(\phi^\dagger\phi)^2. \tag{3.14}$$

This yields an example of a potential giving rise to a second order phase transition which are characterized by a continuous growth of $|\phi|$ with decreasing T, for first order phase transitions this parameter has a discontinuous jump through tunneling. We can see this dynamic by inspecting the potential (3.14): the VEV is $\langle\phi\rangle = 0$ whenever the temperature is greater than some critical value $T > T_c = \sqrt{6}\eta$ while it takes the value $\langle\phi\rangle = \frac{1}{\sqrt{6}}(T_c^2 - T^2)^{1/2}$ for $T < T_c$. Note that at low temperature $\langle\phi\rangle \sim \eta$, this dependence is expected on dimensional grounds and is very generic, recall that $\mu \sim \eta^2$ hence the cosmic string tension can give us very valuable information about the critical temperature associated with a phase transition in the very early universe. Strings are created when the universe has cooled down so that the temperature drops below T_c, at that time ϕ starts rolling towards the new minimum. However in causally disconnected regions, the direction taken by ϕ will be uncorrelated and hence non trivial windings of the field configuration on the vacuum manifold are expected to arise with probability of order one. For instance, with a power-law

expansion the Hubble radius is $H^{-1} \propto t$, therefore we expect at least one cosmic string to be produced per Hubble volume. This gives an lower bound to the number of formed strings: the values of ϕ might be uncorrelated on a smaller length scale $\xi(t)$ and this correlation length must be smaller than the causality bound at all times $\xi(t) < t$. This explanation of the inevitable formation of cosmic strings given a suitable vacuum manifold is called the Kibble mechanism [55]. Figure 3.5 shows a sketch of the situation.

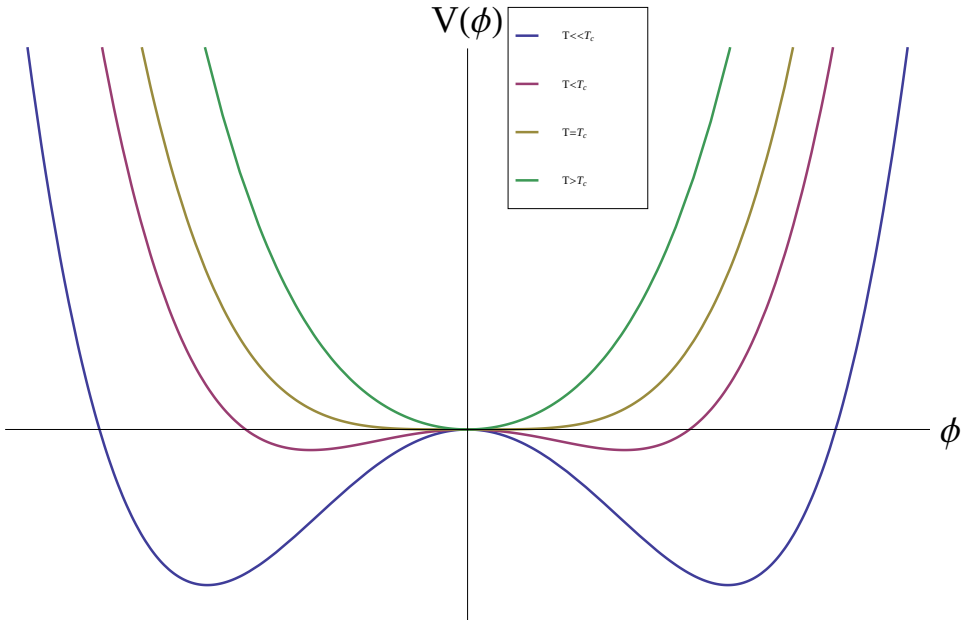

Figure 3.4: Sketch of effective potential at various temperatures.

3.3 Network and Dynamics

After their creation, the strings form a complex and dense network which evolves, through interactions between strings and the expansion of the universe, towards a scaling solution which states its properties become constant in time if all lengths are scaled to the Hubble radius [56]. The network is composed of two parts. The first is the long strings defined by their curvature radius being of the order of the Hubble scale, i.e. $R_c = \gamma t$ with $\gamma \sim \mathcal{O}(1)$. These long strings are assumed to be

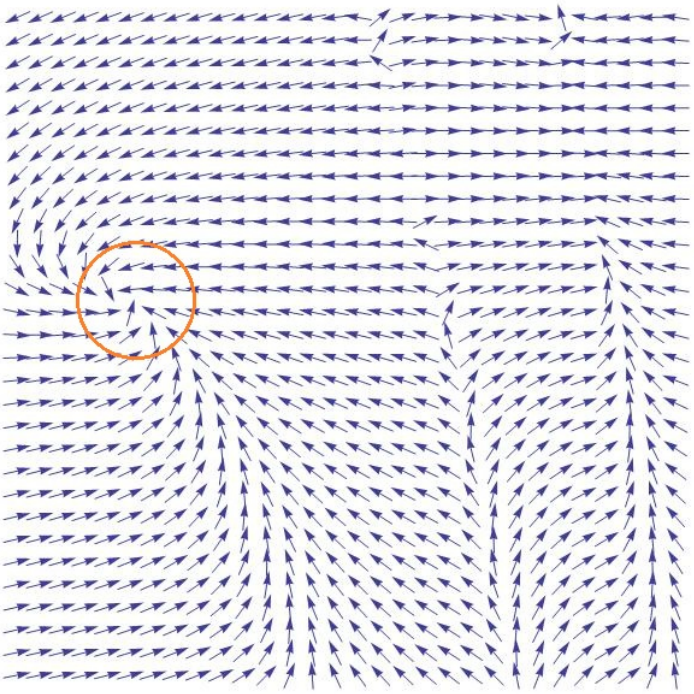

Figure 3.5: Formation of cosmic strings through the Kibble mechanism. The phase of ϕ is uncorrelated on large scales while they tend to align on smaller scales. Such alignment cannot happen in the regions where the winding number is non-zero, as circled in orange, and hence a stable configuration where the field must depart from the vacuum manifold is formed.

straight since any wiggles would either be redshifted away or would cause string self-intersections hence creating string loops that would detach from the mother string thereby straightening it out. This brings us to the second part of the network: a distribution of string loops with curvature radius much smaller than the Hubble scale. To give a quantitative argument for this we must understand the dynamics of cosmic strings.

3.3.1 Dynamics of a Cosmic String

The first thing to note is that if the radius of curvature R of the string is much larger than its thickness δ then we can treat it as a one-dimensional object. Such object will sweep a world sheet described by two coordinates $\zeta^0,\ \zeta^1$. Its spacetime coordinates will depend on the two parameters of the string's worldsheet, namely $x^\mu = x^\mu(\zeta^0, \zeta^1)$. We can define the induced worldsheet metric γ_{ab} the following way,

$$ds^2 = g_{\mu\nu} x^\mu_{,a} x^\nu_{,b} d\zeta^a d\zeta^b, \quad \gamma_{ab} = g_{\mu\nu} x^\mu_{,a} x^\nu_{,b}, \quad \gamma^{ab}\gamma_{bc} = \delta^a_c, \tag{3.15}$$

where the notation $x^\mu_{,a} = \frac{\partial}{\partial x^a} x^\mu$ is used. Since a gauge string has no long range interactions, we can write down a local action to describe its behavior,

$$S = \int \mathcal{L}\sqrt{-\gamma} d^2\zeta, \tag{3.16}$$

where γ is the determinant of the induced metric. The Lagrangian $\mathcal{L}$ can be constructed from the string's tension and geometric quantities such as the extrinsic and intrinsic worldsheet curvature. Moreover we require invariance under spacetime diffeomorphism $x^\mu \to x'^\mu(x^\nu)$ and world sheet reparametrization $\zeta^a \to \zeta'^a(\zeta^b)$. Since we are considering strings with typical radius $R >> \delta$, the tension $\mu \geq \delta^{-2} \gg R^{-2}$ will be much more important than any curvature terms. Hence our Lagrangian can be written as $\mathcal{L} \simeq -\mu$ and then our dynamics is described by the well known Nambu action for one dimensional relativistic strings,

$$S = -\mu \int \sqrt{-\gamma} d^2\zeta. \tag{3.17}$$

Using $d\gamma = \gamma\gamma^{ab} d\gamma_{ab}$ and the Christoffel symbol $\Gamma^{\mu}_{\mu\rho} = \frac{1}{2} g^{\mu\tau}(g_{\tau\nu,\sigma} + g_{\tau\sigma,\nu} - g_{\nu\sigma,\tau})$ we can write down the EOM

$$\frac{1}{\sqrt{-\gamma}} \partial_a \Big(\sqrt{-\gamma} \gamma^{ab} x^{\mu}_{,b} \Big) + \Gamma^{\mu}_{\nu\rho} \gamma^{ab} x^{\nu}_{,a} x^{\nu}_{,b} = 0. \tag{3.18}$$

To simplify our above equation we shall choose to work with a specific gauge called the conformal gauge, namely we determine a specific parametrization of our world sheet by the property that $\gamma_{01} = 0$ and $\gamma_{00} + \gamma_{11} = 0$. The gauge inherits its name since the induced metric takes the conformally flat form $\gamma_{ab} = \sqrt{-\gamma}\eta_{ab}$. However, there is still gauge freedom left, enough so that we can choose $\zeta^0 = x^0 = t$, while $\zeta^1 = \zeta$ becomes a spacelike parameter on the string. This allows us to write the string trajectory as a three vector $\mathbf{x}(\zeta, t)$ which, using $\gamma_{ab} = g_{\mu\nu} x^{\mu}_{,a} x^{\nu}_{,b}$, can be shown to satisfy

$$\dot{\mathbf{x}} \cdot \mathbf{x}' = 0, \tag{3.19}$$

$$\dot{\mathbf{x}}^2 + \mathbf{x}'^2 = 0, \tag{3.20}$$

with $\dot{} = \frac{d}{dt}$, $' = \frac{d}{d\zeta}$. The first equation tells us that the speed of the string is perpendicular to the string's tangent vector. The second can be used to write $d\zeta = (1 - \dot{\mathbf{x}}^2)^{-1/2} |d\mathbf{x}|$ which implies that $d\zeta$ is proportional to the energy of the string since

$$E = \mu \int (1 - \dot{\mathbf{x}}^2)^{-1/2} |d\mathbf{x}| = \mu \int d\zeta. \tag{3.21}$$

If we work in flat spacetime, the Christoffel symbols vanish and the EOM in this gauge is just the wave equation

$$\ddot{\mathbf{x}} - \mathbf{x}'' = 0. \tag{3.22}$$

Therefore any curvature will cause the string to straighten itself out and oscillate. In an expanding background there should also be Hubble friction which makes these

oscillations decay. If we repeat our derivation with a cosmological background using the flat FRW metric $ds^2 = -dt^2 + a(t)^2 d\mathbf{x}^2$, the EOM in equation 3.22 is a bit more complicated and end up being,

$$\ddot{\mathbf{x}} + 2\frac{\dot{a}}{a}(1 - \dot{\mathbf{x}}^2)\dot{\mathbf{x}} = \epsilon^{-1}\Big(\frac{\mathbf{x}'}{\epsilon}\Big)', \tag{3.23}$$

where we chose the $\dot{\mathbf{x}} \cdot \mathbf{x}' = 0$ transverse gauge with the notation (note that now a dot $\dot{}$ refers to a derivative with respect to conformal time $\mathrm{d}\tau = a(\tau)\mathrm{dt}$),

$$\epsilon = \Big(\frac{\mathbf{x}'^2}{1 - \dot{\mathbf{x}}^2}\Big)^{1/2}, \qquad \dot{} = \mathrm{d}/\mathrm{d}\tau, \qquad ' = \mathrm{d}/\mathrm{d}\zeta. \tag{3.24}$$

By using 3.23 and 3.24 we can find the constraint

$$\dot{\epsilon} = -2\frac{\dot{a}}{a}\epsilon\dot{\mathbf{x}}^2,$$

which we use, together with the expression for the energy $E = a(\tau)\mu\int \mathrm{d}\zeta\epsilon$, to get the total rate of change of the string's energy density ρ,

$$\dot{\rho} = \Big(\frac{\dot{a}}{a}\Big)(1 - 2\langle v^2\rangle)\rho, \tag{3.25}$$

where,

$$\langle v^2\rangle = \frac{\int \mathrm{d}\zeta\epsilon\dot{\mathbf{x}}^2}{\int \mathrm{d}\zeta\epsilon}. \tag{3.26}$$

Equation 3.25 describes how a cosmic string will either gain energy through being stretched (first term on the RHS) or lose some by the decay of its velocity/oscillations (second term on the RHS). Both effects are caused by the Hubble flow.

3.3.2 The Long String Network and the Scaling Solution

The string network must be uncorrelated on large scales and hence the shape of long strings follows a random walk beyond a certain scale that we call the characteristic length L of the string network. In other words, in a volume of size L^3, we expect to see ~ 1 string which looks fairly straight. Therefore in a volume V we can estimate

the energy in these long "infinite" strings to be $E = \mu L \frac{V}{L^3}$, or equivalently their energy density $\rho_\infty = \mu/L^2$. If we neglect the damping of sub Hubble "wiggles" on the string (a valid assumption due to the expansion), we can make the approximation that $L(t) = \frac{a(t)}{a(t_i)} L(t_i)$ and hence $\rho_\infty \propto a(t)^{-2}$. This would eventually dominate the energy density of the universe, and cosmic strings would thus suffer the same fate as domain walls. However we have overlooked the possibility that cosmic strings lose energy through loop creation by intersections. Indeed, as mentioned previously, string loops can be created by intersection of two long strings since these have a high probability of exchanging ends after collisions. This process is not fully understood analytically but was shown through numerical simulations. We also are careful in making the assumption that strings are not *superconducting* (there is no electromagnetic current flowing along them) which will be implied from now on, otherwise such strings have a much smaller probability of exchanging ends after intersections.

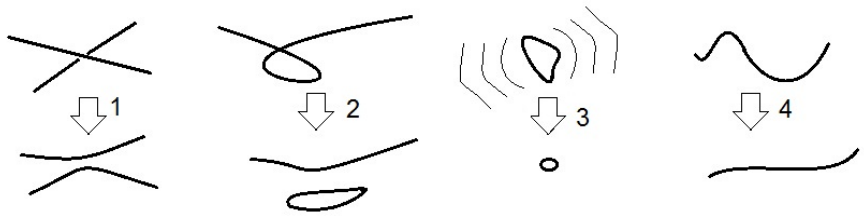

Figure 3.6: Processes involved in string dynamics responsible for the scaling solution. 1) String intersection causes their ends to exchange 2) Self intersections produces string loops 3) Rapid anisotropic oscillations causes the loops to shrink via emission of gravitational radiation 4) Substructures such as "wiggles" on long strings get redshifted away by Hubble expansion.

There is a heuristic picture to understand how string loop production saves the string scenario by changing the scaling of its energy density to an acceptable rate. On average, a string of length L will collide with another string of the same length after having travelling a distance L. Therefore the stationary string in a volume L^3 will get hit by another string after time L hence the rate of collisions per unit volume is L^{-4}. We assume the colliding strings exchange ends to create a loop whose size is

also of the characteristic length. Hence the rate of energy density loss into loops is

$$\dot{\rho}_{loss} \approx \frac{\dot{E}_{loss}}{V} = \frac{1}{V}\frac{\mu L V}{L^4} = \rho_\infty / L, \tag{3.27}$$

so that

$$\frac{\mathrm{d}}{\mathrm{d}t}\rho_\infty \approx -2H\rho_\infty - \frac{\rho_\infty}{L}. \tag{3.28}$$

The characteristic length scale will have a time dependence which describe by $L(t) = \gamma(t)t$. The factor γ allows us to compare how L evolves compared to the horizon length. Plugging this in equation 3.28 along with $\rho_\infty = \mu/L^2$ we find, in the radiation era ($H = 1/2t$),

$$\frac{\dot{\gamma}}{\gamma} \approx -\frac{1}{2t}(1 - 1/\gamma). \tag{3.29}$$

Therefore $\dot{\gamma} > 0$ for $\gamma < 1$ and $\dot{\gamma} < 0$ for $\gamma > 1$ suggesting a fix point at $\gamma \approx 1$. The string network scales in the same way as the horizon so that the energy density scales as $\rho_\infty \sim \mu/t^2$ and does not come to dominate over radiation or matter! In terms of strings, this scaling solution suggest that we should find $\tilde{N} \approx 1$ long strings per Hubble volume. The conclusion of the existence of a scaling solution is supported by numerical simulations but these find $\tilde{N} \approx O(10)$ (see [57] for recent long-string simulations).

3.3.3 The Loop network

This creation of loops from long strings will create a distribution of loops which possesses a scaling peak of loops with radius $\approx 1/20t$ and a decaying tail of smaller loops [59]. The evolution of the string loop distribution is more elusive than the long string network. Nevertheless we can still get a good analytical idea of what the loop network looks like. We first write down the energy density found in loops which will then allow us to determine their number density.

We define a cutoff length to differentiates between infinite strings and loops. This means that we consider any string of length longer than l_c to be of the infinite type and any string below it to be a loop. This cutoff is usually taken to be comparable to the horizon so that $l_c \sim t$. With this in mind, if we assume that the energy loss of the infinite string network is due to a scale-invariant loop production characterised by the function $f(l/L)$ we can then define the rate of energy density loss to be

$$\dot{\rho}_\infty|_{\text{loops}} = \frac{\mu}{L^3}\int_0^{l_c}\frac{\mathrm{d}l}{L}f(l/L) = c\frac{\rho_\infty}{L}. \tag{3.30}$$

Note that $\mu f(l/L)\mathrm{d}l/L$ represents the energy loss into loops of size $[l, l+\mathrm{d}l]$ per unit time per correlation volume L^3 and c is some constant to be determined that depends on $\langle v^2\rangle$ and the cosmological era (matter or radiation dominated).
Moreover we expect $\langle v^2\rangle \sim 1/2$ since this is the value the points of a static loop possess in flat spacetime. In this case the change in the energy density of loops of length l can be written as

$$\dot{\rho}_L(l,t) = -3\Big(\frac{\dot{a}}{a}\Big)\rho_L(l,t) + g\frac{\mu}{L^4}f(l/L), \tag{3.31}$$

with $g = (1-v_i^2)^{1/2} \sim 1/\sqrt{2}$ is a Lorentz factor characterizing the initial speed of the loops. The first term on the RHS describes the redshift of the loop population and the second one takes into account loop creation. This can be integrated to yield, during the radiation epoch,

$$\rho_L(l,t) = \frac{g\mu}{\gamma^{5/2}t^{3/2}l^{3/2}}\int_{l/\gamma t}^{\infty}\mathrm{d}x\sqrt{x}f(x). \tag{3.32}$$

Defining $\nu_r = g\gamma^{-5/2}\int_0^\infty \mathrm{d}x\sqrt{x}f(x)$ we have, at late times,

$$\rho_L(l,t) = \frac{\mu\nu_r}{(tl)^{3/2}}. \tag{3.33}$$

A similar analysis allows us to find the corresponding energy density during the matter dominated era,

$$\rho_L(l,t) = \frac{\mu\nu_m}{t^2 l}, \tag{3.34}$$

with $\nu_m = g\gamma^{-3}\int_0^\infty \mathrm{d}x f(x)$. Note that $f(x),\ g,\ \gamma,\ c$ does not have to be of the same form during the radiation or matter dominated era and we have also left their values undetermined, expressing our ignorance in the dynamics of loop creation.

The above analysis of ρ_L did not take into account the shrinking due to gravitational radiation. Loops are quite asymmetric and have non vanishing quadrupole moment as they oscillate. A loop of length l will decay as $\mathrm{d}l/\mathrm{d}t = -\Gamma G\mu$ [53] with $\Gamma \approx 100$ [59] being a number determined from numerical simulations. Hence a loop of initial length l_i formed at t_i will have at time $t > t_i$ a length,

$$l = l_i - \Gamma G\mu(t - t_i).$$

Modifying our previous work to take into account the shrinking, we simply substitute l_i in terms of t and l in equations 3.33 and 3.34 (we also assume that $t \gg t_i$). If we make the final assumption that all loops are created at the same relative size $l = \alpha t$ - this is the scaling peak we see in numerical simulations with $\alpha \approx 0.05$ - then $f(x) = c\delta(x - \alpha/\gamma)$. Finally, since $\rho_L(l,t) = l\mu n(l,t)$, we find that the number density of loop of length $l < \alpha t$ at time t is,

$$n(l,t) = \frac{\nu_r}{t^{3/2}(l + \Gamma G\mu t)^{5/2}} \tag{3.35}$$

where

$$\nu_r = g\sqrt{\alpha}\gamma_r^{-2}(1 - \langle v_r^2\rangle).$$

Similarly, for loops created in the matter dominated era we have,

$$n(l,t) = \frac{\nu_m}{t^2(l + \Gamma G\mu t)^2} \tag{3.36}$$

$$\nu_m = \frac{2}{3}g\gamma_m^{-2}(1 - 2\langle v_m^2\rangle).$$

There are two behaviors depending on whether $l > \Gamma G\mu$ or not. Defining the quantity $n_l(t) = l\ n(l,t)$ and using the numerical simulations suggesting that, in the

radiation era, $\nu_r \approx 0.4\gamma^{-2}\alpha^{1/2}$ (see section $9.3 - 9.4$ of [53] for numerical modeling discussion), eq. 3.35 reduces to

$$n_l \sim \gamma^{-2}\alpha^{1/2}(tl)^{-3/2}, \qquad \text{for } l > \Gamma G\mu t \tag{3.37}$$

$$n_l \sim lt^{-4}(\Gamma G\mu)^{-5/2}, \qquad \text{for } l < \Gamma G\mu t. \tag{3.38}$$

Therefore a good approximation is to use equation 3.37 with a cutoff at $l = \Gamma G\mu t$. In this case,

$$\rho_L = \int_{\Gamma G\mu t}^{t} n_l \mu \mathrm{d}l \sim \Big(\frac{\alpha}{\Gamma G\mu}\Big)^{1/2} \frac{\mu}{\gamma^2 t^2},$$

which shows that for $\alpha \gg \Gamma G\mu$ we have more energy in loops than in long strings (recall $\rho_\infty \approx \mu/(\gamma t)^2$). This is the case if we adopt the current picture of $\alpha \approx 0.05$, $\Gamma \approx 100$, and $G\mu \leq 10^{-7}$.

In the matter era, $\nu \approx 0.12\gamma^{-2}$ and so,

$$n_l \sim \nu t^{-2} l^{-1}, \qquad \text{for } l > \Gamma G\mu t, \alpha t_{eq}. \tag{3.39}$$

However for $t_{eq} < t < \Big(\frac{\alpha}{\Gamma G\mu}\Big) t_{eq}$ some of the loops formed during the radiation era survived. Their loop distribution will then redshift like the energy density of matter to give,

$$n_l \sim \frac{\alpha^{1/2}}{\gamma^2 (t_{eq} l)^{3/2}} \Big(\frac{t_{eq}}{t}\Big)^2, \qquad \text{for } \Gamma G\mu t \leq l \leq \alpha t_{eq}. \tag{3.40}$$

Considering only $t > \alpha/(\Gamma G\mu)\ t_{eq}$ then only the loops formed in the matter dominated era will remains and their energy density is then,

$$\rho_L \sim \frac{\nu\mu}{t^2} \ln\Big(\frac{\alpha}{\Gamma G\mu}\Big).$$

3.4 Gravitational Effects of Strings

Cosmic strings are essentially lines of trapped energy density, hence we should expect that they have a gravitational effect on their surrounding. These effects will be small enough that we will be able to understand them through linear gravity.

We decompose the string metric into two parts, $g_{\mu\nu} = \eta_{\mu\nu} + h_{\mu\nu}$ where $\eta_{\mu\nu}$ is the Minkowski metric and $|h_{\mu\nu}| \ll 1$ is a small correction. The Einstein equations allow us to determine how matter affects the curvature of spacetime. They are quite hard to solve in general and in order to simplify our lives, it is useful to pick a specific gauge that allow us to put them in a more manageable form. In general relativity (GR) we parametrize spacetime by coordinates x^μ, however the definition of these is arbitrary, we could have chosen a different set of coordinates by performing a coordinate diffeormorphism and instead use $\tilde{x}^\mu = x^\mu + \xi^\mu(x)$ without affecting the physics. Fixing a gauge means fixing which coordinate system we would like to use. In linear gravity, the harmonic gauge is specified by,

$$\partial_\nu \Big(h^\nu_\mu - \frac{1}{2}\delta^\nu_\mu h^\sigma_\sigma \Big) = 0, \tag{3.41}$$

and allows us to write the Einstein equations in a form similar to the wave equation,

$$(\partial_t^2 - \vec{\nabla}^2) h_{\mu\nu} = \Box h_{\mu\nu} = -16\pi G S_{\mu\nu}, \tag{3.42}$$

with,

$$S_{\mu\nu} = T_{\mu\nu} - \frac{1}{2}\eta_{\mu\nu} T^\sigma_\sigma, \tag{3.43}$$

being the source term written in terms of the stress energy tensor $T_{\mu\nu}$, a quantity we can find using the Nambu action for our string.

$$T^{\mu\nu} = \frac{-2}{\sqrt{-g}} \frac{\delta S}{\delta g_{\mu\nu}} = \frac{\mu}{\sqrt{-g}} \int d^2\sigma \sqrt{-\gamma} \gamma^{ab} \frac{\delta \gamma_{ab}}{\delta g_{\mu\nu}} \tag{3.44}$$

$$= \frac{\mu}{\sqrt{-g}} \int d^2\sigma \sqrt{-\gamma} \gamma^{ab} x^\mu_{,a} x^\nu_{,b} \delta^{(4)}(x - x(\sigma)), \tag{3.45}$$

$$T^{\mu\nu}(\mathbf{x}, t) = \mu \int d\sigma (\dot{x}^\mu \dot{x}^\nu - x'^\mu x'^\nu) \delta^{(3)}(\mathbf{x} - \mathbf{x}(\sigma, t)). \tag{3.46}$$

In the last line we have used our gauge freedom on the string worldsheet to write our action in the conformal gauge.

String Loop Metric

We will first attempt to find the metric of a string loop, a harder task than for the long string case. The difficulty with loops is they can oscillate and change their shape frequently and hence change their stress-energy tensor drastically, however this is nothing that averaging cannot cure. Consider a loop centered at the origin and lets look at its retarded time contribution at radius $\mathbf{r}$. The time component of the source $S_0^0 = (T_0^0 - T_i^i)/2$ is,

$$S_0^0(\mathbf{r}, t) = \mu \int d\sigma \dot{\mathbf{x}}^2 \delta^{(3)}(\mathbf{r} - \mathbf{x}(\sigma, t)), \tag{3.47}$$

and the retarded solution of the Einstein equations is,

$$h^{\mu\nu}(\mathbf{r}, t) = -4G \int \frac{d^3y}{|\mathbf{r} - \mathbf{y}|} S^{\mu\nu}(\mathbf{r}, \tau), \tag{3.48}$$

with $\tau = t - |\mathbf{r} - \mathbf{y}|$ being the retarded time. Using $T^{\mu\nu}$ plus the definition of $S^{\mu\nu}$ we integrate over y,

$$h^{\mu\nu}(\mathbf{r}, t) = -4G\mu \int d\sigma \frac{F^{\mu\nu}(\sigma, \tau)}{|\mathbf{r} - \mathbf{x}(\sigma, \tau)|(1 - \mathbf{n} \cdot \dot{\mathbf{x}}(\sigma, \tau))}, \tag{3.49}$$

$$F^{\mu\nu}(\sigma, \tau) = \dot{x}^\mu \dot{x}^\nu - x'^\mu x'^\nu + \eta^{\mu\nu} x'^\sigma x'_\sigma, \tag{3.50}$$

here $\mathbf{n}$ is a unit vector in the direction of $\mathbf{x}$. We now take the time average, namely we integrate a period of time over which the loop oscillation returns to its original position. This period being half of the loop's length [53],

$$\langle h^{\mu\nu}(\mathbf{r}) \rangle = -\frac{8G\mu}{L} \int_0^{L/2} d\tau \int_0^L d\sigma \frac{F^{\mu\nu}(\sigma, \tau)}{|\mathbf{r} - \mathbf{x}(\sigma, \tau)|(1 - \mathbf{n} \cdot \dot{\mathbf{x}}(\sigma, \tau))} \tag{3.51}$$

$$= -\frac{8G\mu}{L} \int_0^{L/2} d\tau \int_0^L d\sigma \frac{F^{\mu\nu}(\sigma, \tau)}{|\mathbf{r}|} \qquad \text{at large } \mathbf{r} \tag{3.52}$$

$$= -\frac{A^{\mu\nu}}{r}. \tag{3.53}$$

With $A^{\mu\nu}$ obtained by performing the integrals over $\tau,\ \sigma$ one obtains the following values,

$$A^{00} = 4G\mu L\langle \dot{\mathbf{x}}^2 \rangle = 2GM, \quad \text{since } \langle \dot{\mathbf{x}}^2 \rangle = 1/2, \tag{3.54}$$

$$A^{0i} = 0, \tag{3.55}$$

$$A^{ij} = 2GM\delta^{ij}. \tag{3.56}$$

So finally we end up with the Scharzschild metric! Far away, and on large enough time scales, an oscillating loop will give rise to a spherical source of mass M. These will be great seeds for structure formation in the early universe.

Straight String Metric

In the case of the long strings we will be interested in studying segments that are shorter than the characteristic length scale of the network, therefore we can restrict ourselves to straight strings. The stress-energy tensor for a straight string lying on the z-axis is,

$$T^{\mu}_{\nu} = \mu\delta(x)\delta(y)diag(1,0,0,1)^{\mu}_{\nu}, \tag{3.57}$$

which allows us to easily solve for $h_{\mu\nu}$ to find,

$$h_{00} = h_{33} = 0,\ h = h_{11} = h_{22} = 8G\mu \ln\Big(\frac{r}{r_0}\Big), \tag{3.58}$$

with $r = (x^2 + y^2)^{1/2}$ and r_0 an integration constant. This yields the following metric,

$$ds^2 = dt^2 - dz^2 - (1-h)(dr^2 + r^2 d\theta^2). \tag{3.59}$$

Our linear approximation seems to break down for large r but this is just due to a poor choice of coordinates, letting $(1-h)r^2 = (1-8G\mu)r'^2$ we can rewrite the

metric to linear order in $G\mu$ as,

$$ds^2 = dt^2 - dz^2 - dr'^2 - (1 - 8G\mu)r'^2 d\theta^2 \tag{3.60}$$

$$= dt^2 - dz^2 - dr'^2 - r'^2 d\theta'^2, \tag{3.61}$$

with $\theta' = (1 - 4G\mu)\theta$. So locally this is just a flat spacetime! Hence a straight cosmic string will not have a gravitational pull associated to it; the non-trivial effect of the long strings will come due to this redefinition of the angle. If we look at the geometry more closely, we see that spacetime is actually conical with the tip at the string. Indeed, $0 \leq \theta' \leq 2\pi(1-4G\mu)$ so we define the deficit angle $\triangle = 8\pi G\mu$. How can this global feature of our spacetime can affect the dynamics of test particles? Consider figure 3.7, the string is in the middle and we have drawn the trajectory of two test particles. As the string moves between them, we observe they start to move towards one another. Therefore if the string moved in a gas of particles initially at rest, a static observer residing in the plane swept by the string would see particles acquire a velocity kick **towards** him as the string passed by. The magnitude of the impulse is

$$v = 4\pi G\mu v_s \gamma_s, \tag{3.62}$$

where v_s is the velocity of the string and γ_s is the corresponding gamma factor that arise from being in the rest frame.

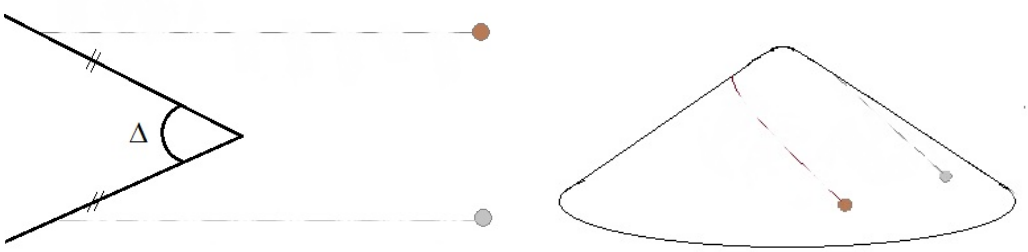

Figure 3.7: (Left) The conical deficit created by the string is shown, the lines marked by two slash (//) should be identified. We draw the dashed trajectories of two test particles. They eventually meet. (Right) We draw the same situation on the left hand side after removing the deficit angle. Note that the ambiguity in the direction of the cut made on the left disappears. Also the tip of the cone is smoothed out because of the string's width. In the case of a global string - with "infinite" width - the divergent energy density would force the deficit angle to increase as we moved away from the string's location and eventually the universe would close back on itself.

4

Structure Formation from Loopy Strings

4.1 The Zel'dovich approximation

We want to understand how a string accretes matter. For this, we introduce the Zel'dovich approximation [61], a method that allows us to calculate trajectories of particles with good approximation even as they enter some non-linear regime. The idea behind the technique is to choose a Lagrangian frame which follows the bulk flow of the fluid, in contrast to an Eulerian frame who is kept at a fixed spatial position. To follow the evolution of dark matter particles using this technique, hence consider such particles described by trajectories in an expanding FRW background

$$\mathbf{r}(\mathbf{x}, t) = a(t)[\mathbf{x} + \mathbf{\Psi}(\mathbf{x}, t)].$$

Here $\mathbf{x}$ and $\mathbf{\Psi}$ represents the unperturbed comoving position and the comoving displacement from that position respectively and $a(t)$ is the scale factor. The physical coordinate $\mathbf{r}$ has as equation of motion,

$$\ddot{\mathbf{r}} = -\nabla_r \mathbf{\Phi}, \tag{4.1}$$

for a gravitational potential $\Phi(\mathbf{r}, t)$ satisfying the Poisson equation $\nabla_r^2 \mathbf{\Phi} = 4\pi G(\rho_s + \rho)$. Here $\rho(\mathbf{r}, t)$ is the dark matter density while $\rho_s(\mathbf{r}, t)$ is the density of the string seed. Introducing a new coordinate system with $\mathbf{r}$ we can then define $\rho(\mathbf{r}, t)$, through

mass conservation $\rho_{av}a^3d^3x = \rho(\mathbf{r},t)d^3r$, by

$$\rho(\mathbf{r},t) = \frac{\rho_{av}(t)a^3(t)}{|\det(\partial\mathbf{r}/\partial\mathbf{x})|}, \tag{4.2}$$

$$\approx \rho_{av}(t)[1 - \nabla_x \cdot \mathbf{\Psi}(\mathbf{x},t)]. \tag{4.3}$$

In the second line we expanded the determinant to first order in $\mathbf{\Psi}$ using $\det(1+A) = 1 + \mathrm{tr}A + \mathcal{O}(A^2)$.

4.2 Accretion unto loops

We now consider the case of a string loop with $\rho_s = m\delta[\mathbf{r} - \mathbf{r}_s(t)]$ in a matter dominated era such that $\rho_{av} = 1/(6\pi G t^2)$. Using this with the Poisson equation for $\mathbf{\Phi}$ we obtain,

$$\nabla_r \mathbf{\Phi} = \frac{4\pi}{3} G\rho_{av}(\mathbf{r} - 3a\mathbf{\Psi}) + \frac{Gm(\mathbf{r} - \mathbf{r}_s)}{|\mathbf{r} - \mathbf{r}_s|^3}.$$

We can now use that expression and the EOM 4.1 to write the linearized equation of motion for the displacement,

$$\ddot{\mathbf{\Psi}} + \frac{4}{3t}\dot{\mathbf{\Psi}} - \frac{2}{3t^2}\mathbf{\Psi} = -\frac{Gm(\mathbf{x} - \mathbf{x}_s)}{a^3|\mathbf{x} - \mathbf{x}_s|^3}, \tag{4.4}$$

with $\mathbf{x}_s = \mathbf{r}_s/a(t)$. Taking the divergence of this equation and noting that $\delta\rho/\rho = -\nabla_x \cdot \mathbf{\Psi}$ we rewrite the equation of motion as

$$\Big(\frac{\partial^2}{\partial t^2} + \frac{4}{3t}\frac{\partial}{\partial t} - \frac{2}{3t^2}\Big)\frac{\delta\rho}{\rho}(\mathbf{x},t) = \frac{4\pi G m}{a^3(t)}\delta[\mathbf{x} - \mathbf{x}_s(t)].$$

For $m = 0$ the solution is $\delta\rho/\rho = A(\mathbf{x})t^{2/3} + B(\mathbf{x})t^{-1}$, which is the usual result from linear perturbation theory. Moreover if $\delta\rho/\rho = 0$ and a loop seed is introduced, then the perturbations will stay zero outside the loop.

4.2.1 Static Loops

Since matter perturbations do not grow until t_{eq} we can focus on computing the accreted mass on a loop formed at $t_i > t_{eq}$. The initial conditions of a particle's

displacement $\mathbf{\Psi}$ is $\mathbf{\Psi}(\mathbf{x}, t_i) = \dot{\mathbf{\Psi}}(\mathbf{x}, t_i) = 0$ with $a(t_i) = 1$. Then from the equation 4.4 with a loop seed of mass m, we find the solution,

$$\mathbf{\Psi}(\mathbf{x}, t) = \frac{3Gm\mathbf{x}t_i^2}{2|\mathbf{x}|^3}\Big[1 - \frac{2}{5}\Big(\frac{t_i}{t}\Big) - \frac{3}{5}\Big(\frac{t}{t_i}\Big)^{2/3}\Big], \tag{4.5}$$

$$\approx -\frac{9}{10}\frac{Gm\mathbf{x}t_i^2}{|\mathbf{x}|^3}\Big(\frac{t}{t_i}\Big)^{2/3} \qquad \text{for } t \gg t_i. \tag{4.6}$$

The turnaround surface is the given by $\dot{\mathbf{r}} = 0$ yielding the following expression for the radius of the turnaround sphere at time t,

$$|\mathbf{x}|^3 = \frac{9}{5}Gmt_i^2\Big(\frac{t}{t_i}\Big)^{2/3}. \tag{4.7}$$

In such conformal coordinates, the mass enclosed by a sphere of initial radius $r_i = a(t_i)|x|$ is simply $(4\pi/3)\rho_i|x|^3$. Hence the mass falling towards the perturbation at time t is $M = \frac{2}{5}m(t/t_i)^{2/3}$ and the sphere has a radius

$$r_{max} = a(t)r_i = \frac{5}{2}\Big(\frac{3}{4\pi}\frac{m}{\rho_i}\Big)^{1/3}\Big(\frac{M}{m}\Big)^{4/3}. \tag{4.8}$$

Using equation 4.8 and $\mathrm{d}M/\mathrm{d}r = 4\pi r^2\rho$ shows that we end up with a radial density profile following $\rho \propto r^{-9/4}$. The finite size of the loop $L \sim m/\mu$ was neglected and would initially enclose a mass of $M_L \sim \rho_i L^3$ inside the loop. Hence our analysis should only be valid for $M > M_L$ which corresponds to a turnaround radius of $r > L^3/(G\mu t_i^2)$.

4.2.2 Moving Loops

Now lets turn to the accretion pattern created by a moving loop. We must first determine the loop trajectory. This can be achieved from the equation of motion 4.1 of a point charge, namely $\ddot{\mathbf{r}} = \frac{-4\pi G}{3}\rho_{avg}\mathbf{r}$, here we denote the average density of the universe by ρ_{avg}. Using the second Friedmann equation $\ddot{a}/a = (-4\pi G/3)\rho_{avg}$ and that $\mathbf{r} = a\mathbf{x}$ we can find the motion of the loop. Suppose it starts at $\mathbf{r_s} = 0$, has an initial velocity $\mathbf{v_i}$ at t_i, and is accelerating with the Hubble flow, then using

the EOM and Friedmann's equation,

$$\ddot{\mathbf{r}} = \ddot{a}\mathbf{x} + 2\dot{a}\dot{\mathbf{x}} + a\ddot{\mathbf{x}} = \ddot{a}\mathbf{x}, \tag{4.9}$$

and since $a \propto t^{2/3}$,

$$2H\dot{\mathbf{x}} + \ddot{\mathbf{x}} = 0 \rightarrow \frac{dv}{v} = -\frac{4}{3t}, \tag{4.10}$$

integrating and using the initial conditions,

$$\mathbf{x} = 3\mathbf{v}_i t_i (1 - a^{-1/2}), \tag{4.11}$$

and hence $\mathbf{x}_s(t) = 3\mathbf{v}_i t_i(1 - a^{-1/2}) \equiv d(1 - a^{-1/2})\hat{e}_z$ with the last equality being for a loop moving strictly in the z-direction with $d = 3v_i t_i$. The solution to equation 4.4 with the above initial conditions was found by Bertschinger [60] to be (for $t \gg t_i$ and neglecting the decaying mode),

$$\mathbf{\Psi}(\mathbf{x}, t) = -b(t)d[\hat{e}_x f_x(\mathbf{x}) + \hat{e}_z f_z(\mathbf{x})], \tag{4.12}$$

where

$$b(t) = \frac{1}{5}\frac{Gm}{v_i^2 d}a(t), \tag{4.13}$$

$$f_x = \frac{R_f - R_i}{x} + \frac{zd}{xR_i}. \tag{4.14}$$

$$f_z = \ln\left(\frac{R_i + z}{R_f + z - d}\right) - \frac{d}{R_i}, \tag{4.15}$$

$$R_i = (x^2 + z^2)^{1/2}, \qquad \text{distance from } \mathbf{x} \text{ to } \mathbf{x}_s(t_i) = 0 \tag{4.16}$$

$$R_f = (x^2 + (z - d)^2)^{1/2}, \qquad \text{distance from } \mathbf{x} \text{ to } \mathbf{x}_s(t). \tag{4.17}$$

The turnaround surface in this case is defined as the surface such that $\dot{r}_x = 0$ with $\mathbf{r} = a[\mathbf{x} + \mathbf{\Psi}]$. This yields the condition $x + 2\Psi_x = 0$ and we obtain

$$x = 2db(t)f_x(x, z). \tag{4.18}$$

At late time the surfaces are nearly spherical and we find that $\mathbf{f} \approx \frac{d}{2(x^2+z^2)}\mathbf{e}_r$, however at early times the accreted matter resides in a thin band behind the loop and therefore we can expand 4.18 for $x^2 \ll z^2, (d-z)^2$ which yields

$$x^2 = 4b(t)d(d-z). \tag{4.19}$$

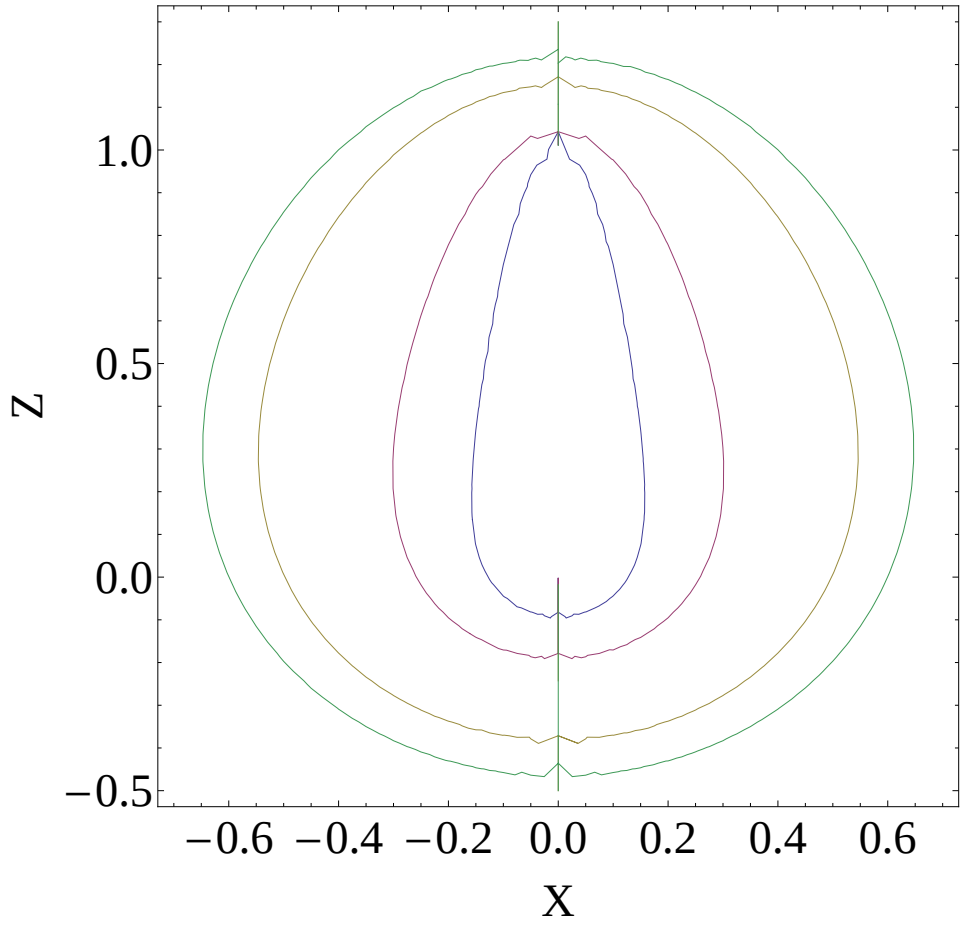

Figure 4.1: The turnaround surfaces around a moving string loop. The curves corresponds to the contour plots of eq. 4.18 for different values of t. Early on, the surfaces form a thin band behind the loop and become progressively more spherical as time progresses.

The accreted mass can be estimated by integrating over the narrow turnaround

surface

$$M \approx \rho_i \int_0^d \pi x^2 dz = \frac{3}{5} m \Big(\frac{t}{t_i}\Big)^{2/3}, \tag{4.20}$$

which is found to be of the same order as the case of a static loop and is also independent of the loop's initial velocity. For large and slow loops, their motion will be affected by the drag caused by the accretion of matter in their wakes, however since most loops are formed on small scales with high velocity they decay before this effect becomes important. Moreover there is also the gravitational rocket effect - the oscillations on the loop produces gravitational waves that accelerates the loop in some random direction $\hat{\mathbf{n}}$ - and therefore the loops trajectory should be curved but this is not important when determining the structures it forms [32].

Knowing the loop distribution from the scaling solution and the dynamics of mass accretion, the number and properties of dark matter halos obtained from these objects was studied by Schlaer et al. [32]. The mass accreted by moving loops will form an elongated cylinder that will fragment in smaller beads due to gravitational instability. Hence there will be more halos than loops. Moreover, for strings with $G\mu \geq 10^{-7}$, [32] found that a significant amount of star forming halos could be produced at early times. These could have a detectable impact on the period of reionization.

Such results motivates studying the contribution to structure formation from the second part of the string network, namely the long strings. The rest of the thesis will address this question.

5

Structure Formation from Long Strings

5.1 Accretion unto wakes

Here we also make use of the Zel'dovich approximation to study the accretion of matter behind the long straight strings. Recall that due to the conical deficit, the effect of the moving string on the surrounding particles will be to induce a kick in the direction perpendicular the plane that they sweep, giving them a speed of $v = 4\pi G\mu v_s\gamma_s$ where v_s is the speed of the string and γ_s is the corresponding gamma factor that arises from being in the rest frame of the wake. Other than that, the string has no gravitational effect on the surrounding gas. However this kick will cause an overdensity of matter to form behind the string (see figure 5.1), gravitational instability will set in and matter starts pilling up and decoupling from the Hubble flow in the dimension transverse to the string's worldsheet. These non-linear objects, that we call the strings wakes, are formed as soon as matter perturbations can start growing, namely at t_{eq}. The goal of this thesis is to understand what kind of structures can be formed from those. We first determine the dynamics of the wakes formation and evolution.

Consider a particle that finds itself above the plane swept by the string and label its distance from the wake by $r = a(t)(x + \psi)$. We can then find the particle's trajectory from the equation of motion obtained as in section 4.2,

$$\ddot{\psi} + \frac{4}{3t}\dot{\psi} - \frac{2}{3t^2}\psi = 0 \tag{5.1}$$

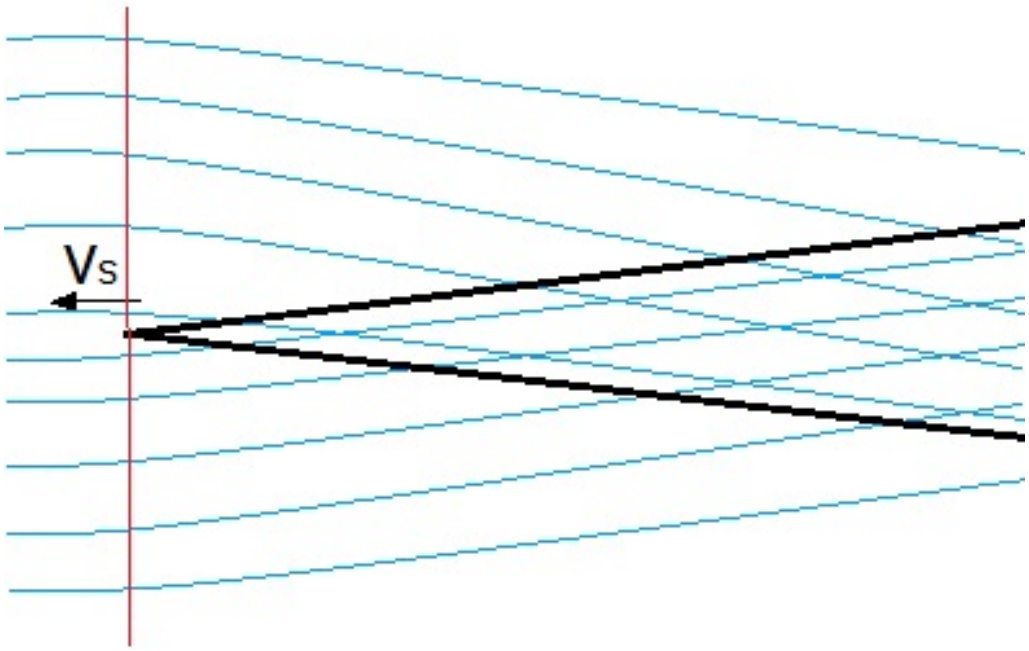

Figure 5.1: Particles receive a kick as a long cosmic strings moves through the gas. The streams overlap and creates an overdensity of matter. The string extends outside of the page and the red line denotes the position where particles experiences the impulse.

with initial condition $\dot{\psi}(x,t_i) = -\mathrm{sgn}(x)v$, $\psi(x,t_i) = 0$. The solution to this equation is

$$\psi(x,t) = -\frac{12}{5}G\mu\pi v_s\gamma_s t_i\Big(\frac{t}{t_i}\Big)^{2/3} + \frac{12}{5}G\mu\pi v_s\gamma_s\frac{t_i^2}{t}. \tag{5.2}$$

Dropping the decaying mode corresponding to the second term, we can find the turnaround surface from the condition $\dot{r} = 0$ or more specifically $x + 2\psi = 0$ which yields,

$$x(t) = \pm\frac{24}{5}G\mu\pi v_s\gamma_s t_i\Big(\frac{t}{t_i}\Big)^{2/3}. \tag{5.3}$$

This shows that the turnaround surface happens at a comoving distance that is half of what it should have been without the wake ($x_{ta} = \frac{1}{2}x(t)$). Moreover the physical width of the wake will be given by $w(t) = 2r_{ta}(t) = x(t)\frac{a(t)}{a(t_i)}$ and the surface density will simply be $\sigma(t) = w2\rho_{avg}$. Explicitly these are,

$$w(t) = \frac{24}{5}\pi G\mu v_s\gamma_s t_i\Big(\frac{t}{t_i}\Big)^{2/3}\Big(\frac{t}{t_i}\Big)^{2/3} = \frac{6}{5}vt_i\Big(\frac{t}{t_i}\Big)^{4/3}, \tag{5.4}$$

$$\sigma(t) = \frac{2v}{5\pi G t}\Big(\frac{t}{t_i}\Big)^{1/3} \tag{5.5}$$

$$= \frac{8\pi G\mu v_s\gamma_s}{5\pi G t_0}(z+1)^{3/2}\Big(\frac{z_i+1}{z+1}\Big)^{1/2}. \tag{5.6}$$

This behavior makes sense at an intuitive level. Since the area of the sheet grows with the scale factor as $\sim a^2$, the surface density should decrease by the inverse of this, however we know from linear perturbation theory that overdensities grows as $\sim a$ and hence the surface density should only decrease as $\sim a^{-1}$ which is the result. The dimension of these wakes will be approximately $c_1 t_i \times v_s\gamma_s t_i \times 4\pi G\mu v_s\gamma_s t_i$ at time t_i.

5.2 Thermalization, shocks and diffuse wakes

Matter that turned around at a height r_{ta} will virialize at a radius $\frac{1}{2}r_{ta}$ and hence the density of matter in the wake should be 4 times higher than the background. Shells of infalling baryonic matter will collide with one another at that distance and hence will create shocks on either side of the wake. The energy of the falling particle will be thermalized in the wake. The temperature was estimated in [62] by considering the relation

$$\frac{3}{2}k_B T = \frac{1}{2}m v_{shell}^2, \tag{5.7}$$

where v_{shell} is the speed of the shell of hydrogen particles of mass m that collides with the wake to form the shock. A shell that turns around at time t_{ta} will hit the wake at $t = (1+1/\sqrt{2})^{3/2}t_{ta}$, therefore their speed will be given by

$$v_{shell} = \dot{r}(t, t_{ta} = t(1+1/\sqrt{2})^{-3/2}) = \frac{4}{5}(3-2\sqrt{2})v\Big(\frac{t}{t_i}\Big)^{1/3}, \tag{5.8}$$

which yields an average temperature,

$$T = \frac{16}{75}(4(3-2\sqrt{2}))^2\frac{m}{k_B}(G\mu)^2(v_s\gamma_s)^2\Big(\frac{t}{t_i}\Big)^{2/3} \tag{5.9}$$

$$\simeq [10K](G\mu)_6^2(v_s\gamma_s)^2\frac{z_i+1}{z+1}, \tag{5.10}$$

This temperature is actually very low, mainly because gravity is only pulling in one direction. Numerical simulations of the wake [63] agree fairly well with this value. Moreover it is interesting to note that the baryonic and dark matter will not have similar density profiles inside the wake. Since dark matter is nearly collisionless, its density will spike on the edge of the wake at the turnaround point. Baryonic matter will get stuck in the middle by additional matter piling up on it, this is shown in figures 5.2 obtained from the simulation done in [63]. This makes it hard to predict the subsequent dynamics of small perturbations of matter density, which we would need to determine structure formation. We will come back to this point latter.

For the moment, notice that during a long period of time, the background temperature is higher than the wake's. Therefore at high redshifts the thermal velocity should satisfy $v_{th} > v_{shell}$ which means our derivation of the wake's width - from the virial theorem - was not quite right. Before the background's temperature decreases below the wake's, the latter will be diffuse [64].

Until $z \lesssim 150 - 300$ the hydrogen gas in the universe is still coupled to the CMB radiation. The hydrogen temperature T_H will follow the CMB temperature $T_{cmb}(z) = 2.725(1+z)$ until decoupling. Afterwards the hydrogen expand as an adiabatic gas. Since adiabatic processes for monatomic gases can be described by $VT_H^3 = const$ we can use $V \propto a^3$ to determine that $T_H \propto (1+z)^2$ [65]. Obtaining a crude approximation by asking that these two temperature agree at $z = 150$ we find $T_H = \frac{2.725}{150+1}(1+z)^2$. Shocks will be created when $T_{wake}(z_{shock}) = T_H(z_{shock})$. We use our computed T_{wake} to obtain,

$$1 + z_{shock} = \Big(\frac{1510}{2.725}(G\mu)_6^2(v_s\gamma_s)^2(z_i+1)\Big)^{1/3}, \tag{5.11}$$

and hence $z_{shock} \approx 23$ for a wake created at t_{eq} with $G\mu \sim 10^{-7}$, $v_s\gamma_s = 1/\sqrt{3}$.

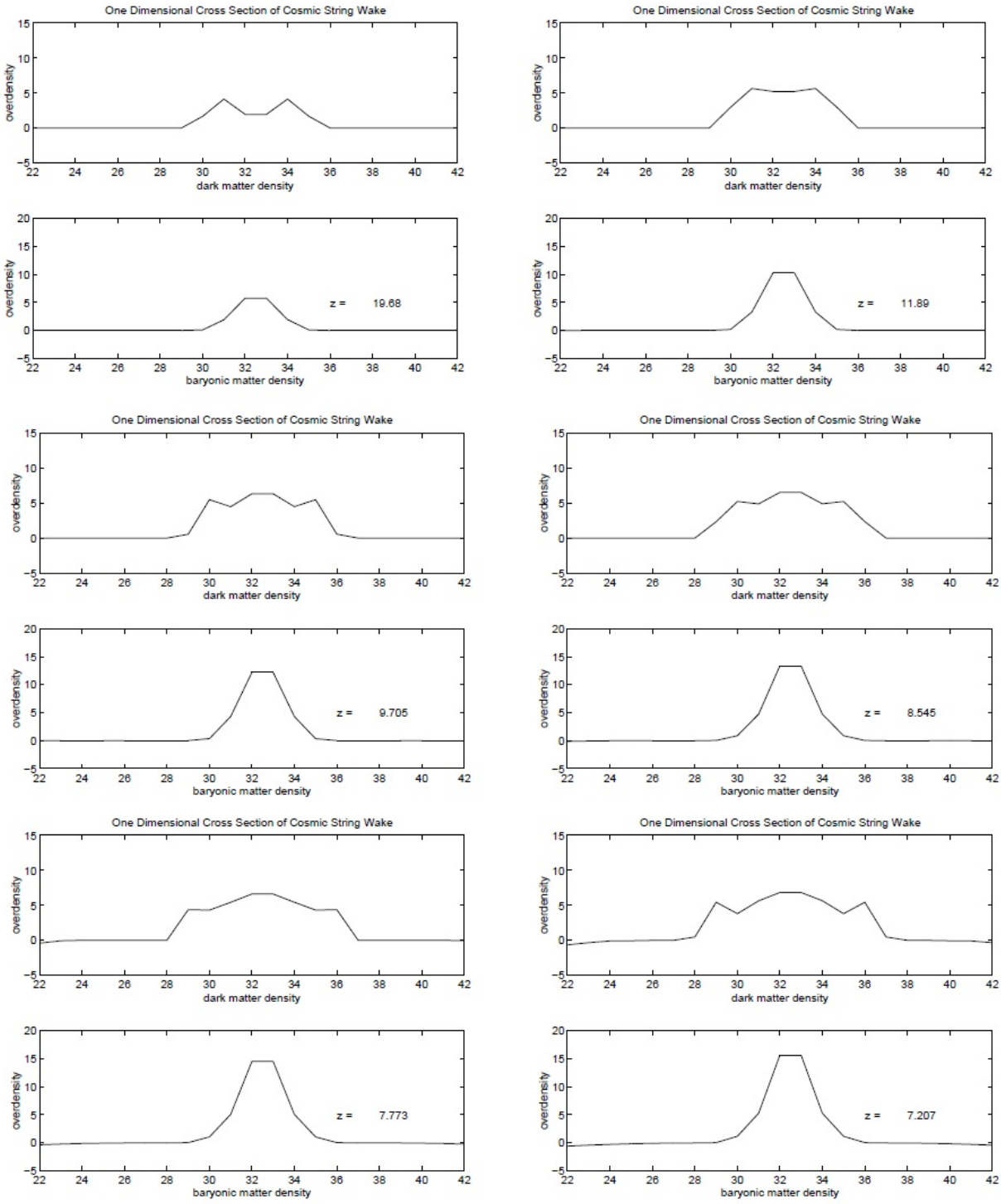

Figure 5.2: Density profile of matter inside the wake at different times. The figures were taken from [63].

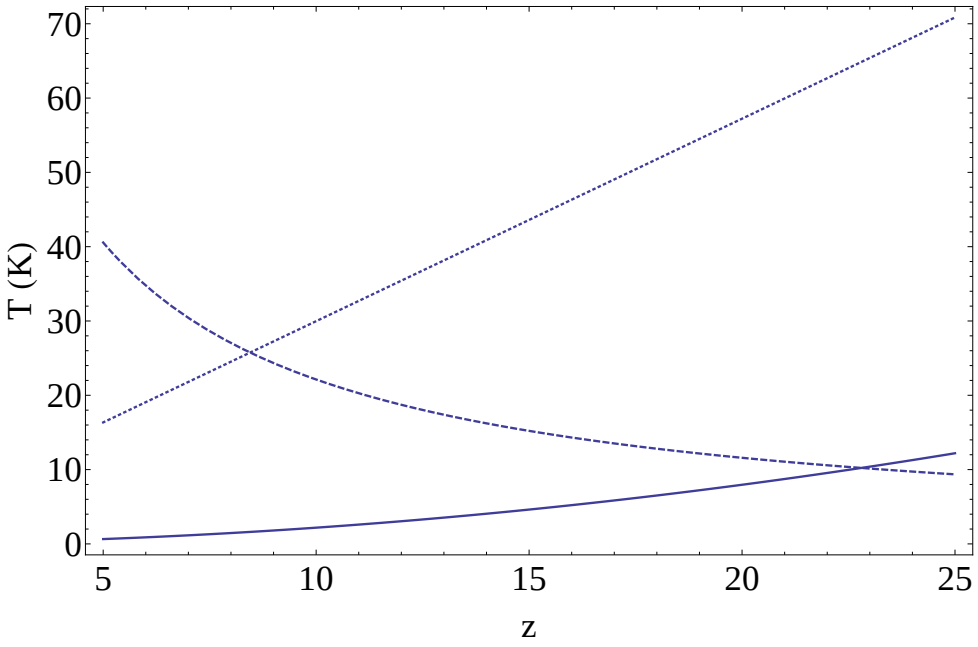

Figure 5.3: Temperature of the wake (dashed), matter (solid) and CMB (dotted) at different redshifts.

5.3 *Fragmentation*

As we previously discussed, the substructure of the wake makes it very hard to accurately predict the dynamics of perturbations without resorting to N-body simulations. We will still attempt to get an idea of what might happen using analytical tools.

Recall that the Newtonian hydrodynamical equations for the growth of a perturbation in a fluid with expanding background is given by

$$\ddot{\delta_k} + 2H\dot{\delta}_k + \left(\frac{c_s^2}{a^2}k^2 - 4\pi G\rho_b\right)\delta_k = 0, \tag{5.12}$$

where δ_k is the Fourier mode with comoving wavenumber k of the density perturbation characterized by $\rho = \rho_b(1+\delta)$. The solutions to this equation depends on the value of k. If $k \ll k_J = \left(\frac{4\pi G\rho_b}{c_s^2}\right)^{1/2}$ we have as solution

$$\delta_k = C_1 t^{2/3} + C_2 t^{-1},$$

which means that the perturbation grows. On the other hand if $k \gg k_J$ the overdensity has an oscillatory behavior. The Jean's length in the wake ends up being

$$\lambda_J = \frac{16\pi}{5}(3-2\sqrt{2})\sqrt{3/2}G\mu v_s\gamma_s\frac{t^{4/3}}{t_i^{1/3}} \sim 2.11 \times G\mu v_s\gamma_s\frac{t^{4/3}}{t_i^{1/3}} \sim w. \tag{5.13}$$

Hence we might expect fragmentation of the wake into blobs of size $\sim w^3$. Another clue that this is the right picture is from a detailed analysis by Miyama et al. [66] of perturbation growth in a *static* isothermal sheet-like cloud. They found that the timescale of perturbation growth is of the order of the freefall time with the length of the most unstable mode equalling the sheet's width and the longest wavelength unstable mode being twice that. Taking the very optimistic route and assuming our wake behaves in a similar way[1], long filaments of virial diameter $\approx w(t)$ should form in a similar fashion to the Zel'dovich pancakes. These filaments would subsequently break into beads themselves, again the fastest growing mode having a length $\approx 2\pi w(t)$ [32]. Therefore the wakes will eventually fragment into virialized halos of size $\approx \pi(w/2)^3$, in agreement with our previous Jean's length analysis. Similar conclusions were also obtained in [67]. We will assume this optimistic picture for the rest of this thesis.

5.4 Properties of Halo's and Star formation

To compute the properties of the clumps formed by wake fragmentation, we assume the dynamics described in [66]. Therefore virialized halos of size $\approx \pi(w(z)/2)^3$ will quickly form at redshift z. These halos will likely have obtained a very clumpy substructure due to their bottom-up hierarchical formation.

[1]The neglect of Hubble flow along the wake might not be justified. In an expanding universe structures with planar, cylindrical and spherical symmetry undergo a self-similar growth proportional to $t^{4/3}$, t and $t^{8/9}$ respectively [68]. In this case one could argue that if perturbations grew as cylindrical or spherical objects, they would grow slower than the planar wake and therefore no clear fragmentation would occur.

The temperature of halos can be estimated from the virial theorem and conservation of energy by considering a collapsing gas cloud of radius w containing two times the background density ρ_0,

$$2\frac{1}{2}v_{virial}^2 = \frac{3}{5}\frac{GM}{r_{virial}}, \tag{5.14}$$

$$\frac{1}{2}v_{virial}^2 - \frac{3}{5}\frac{GM}{r_{virial}} = \frac{1}{2}v_{th}^2 - \frac{3}{5}\frac{GM}{w}, \tag{5.15}$$

with w being the radius of our collapsing cloud, $M = 2\rho_b\frac{4}{3}\pi(w)^3$ its mass and $v_{th} = v_{shell}$ the initial thermal velocity. The shock heated baryonic gas will have a temperature of $T = \frac{\mu}{2}\frac{m_p}{k_b}v^2$, with m_H being the mass of the proton and μ the mean molecular weight [41]. Star formation can occur if the temperatures are high enough so that colliding molecules can excite each other to higher energy states. They will then radiate energy away when they come back to their ground state and hence lose some momentum, sinking in the potential well. Atomic cooling requires $T > 10^4$K while $H2$ cooling has channels that can be efficient to temperatures as low as 200K. However these $H2$ molecules are very fragile and get destroyed by the radiation of the first stars, therefore this cooling mechanism alone will not allow for multiple stars to form in close proximity as would be the case for halos formed from wakes. Figure 5.4 shows the temperature of the hottest halos that can be formed with the parameters in eq. 5.19 and $\mu \approx 1.22$ in the case of neutral hydrogen. As we can see, the temperatures are far too low to have any significant star formation, and hence no noticeable effect on the history of reionization will be present. This will also make the halos essentially invisible to optical telescopes.

5.5 Toy Model for the Long String Network

Now that we've seen what kind of halos are formed from wakes. We can work towards writing down a mass function for the halos. The first step is to must understand the network and distribution of wakes created from our scaling solution. As

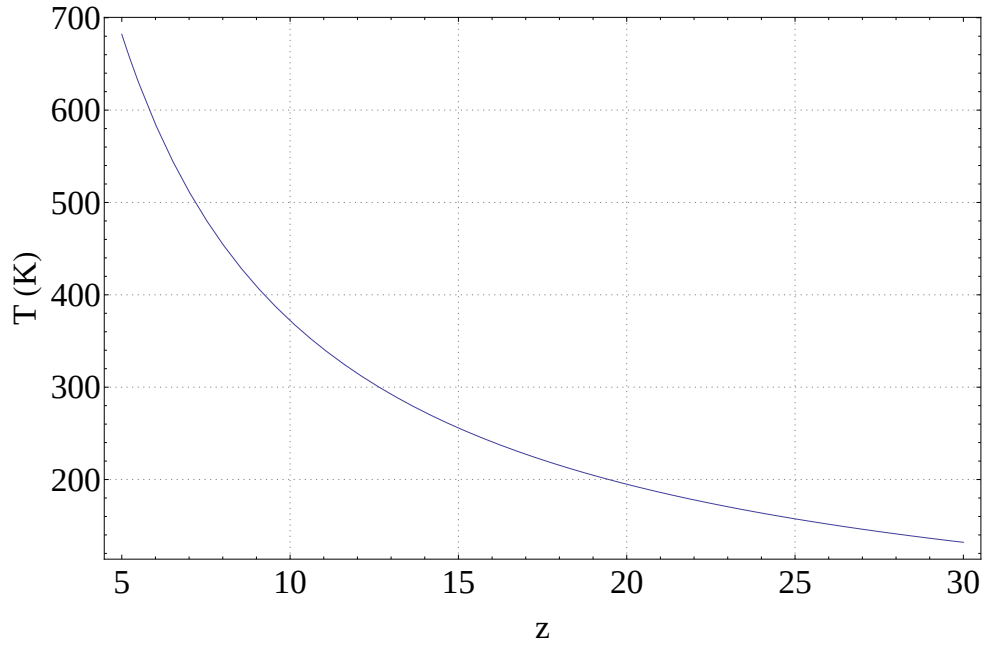

Figure 5.4: Redshift dependence of the temperature in the hottest halos that are formed from wakes. We use the parameters in eq. 5.19 and $\mu \approx 1.22$.

previously mentioned, we expect $\tilde{N}$ strings per Hubble volume which grow in length through expansion of space and can also change their direction of motion after intersecting other strings and exchanging ends. We use a toy model introduced in [70] and used in [71] to characterize these features. Wakes first form behind strings at the time of equal matter-radiation energy density t_{eq}, when matter perturbations can start to grow. Therefore we consider Hubble time steps from t_{eq} to t_0 labelling $t_1 = t_{eq},\ t_2 = 2t_{eq}, ..., t_m = 2^{m-1}t_{eq}$. At the beginning of each time step we create $\tilde{N}$ strings of length γt where γ is less but close to unity and each string has a velocity v_s in a random direction. At the end of the time step we remove them and start over with a new set of strings. At each time steps, every strings will have laid down a wake with dimensions $\gamma t_m \times v_s \gamma_s t_m \times w(t)$ that will then grow from Hubble expansion and matter accretion to eventually fragment as discussed above.

5.6 DM Halo mass function

Consider a redshift z, then the comoving number density of wakes laid down at time $z_m > z$ is given by,

$$\tilde{n}_{wake}(z_m) = \frac{\tilde{N}}{H_m^{-3}} \frac{1}{(z_m+1)^3}. \tag{5.16}$$

Each wake will fragment in clumps of the size of its width. Therefore one can compute the comoving number density of halos of mass greater than M that fragments from the wakes created at redshift z_m:

$$n(z,z_m,>M) = \tilde{n}_{wake}(z_m)\frac{\mathrm{Vol}_{wake}}{\mathrm{Vol}_{halo}}\Theta(M_{halo}-M) \tag{5.17}$$

$$= \tilde{n}_{wake}(z_m)(\gamma t_m \times v_s\gamma_s t_m \times w(z))\Big(\frac{z_m+1}{z+1}\Big)^2 \frac{1}{\frac{4}{3}\pi w(z)^3}\Theta(2\rho_b(z)\frac{4\pi}{3}w(z)^3 - M), \tag{5.18}$$

where Θ is the Heaviside step function

If we want to consider all the wakes that exist at redshift z we simply consider $n(z,>M) = \sum_{z_m>z} n(z,z_m,>M)$. The collection of step functions given by the sum is a bit odd as a distribution since in reality this should be continuous. The discrepancy arises because of the model that considers the wakes to be instantaneously create while this process actually spans a Hubble time. The part of a wake that is being created close to time t_m will have different properties than the part created at around $2t_m$ which will look more like the beginning of the next set of wakes. Hence we should smear out the distribution $n(z,>M)$ to have something more realistic. To do this we fix z and split the mass range in intervals $\Delta M_m = [M(z,z_m), M(z,z_{m-1})]$ with $M(z,z_j)$ being the mass of the halos formed at z from a wake created at z_j being the redshift of our Hubble time steps. Since the values of $n(z,>M(z_j)) = \sum_{m>j} n(z,z_m,>M)$ are known, we can just linearly interpolate to create a continuous $n(z,>M)$. One can then obtain the comoving mass function from $\frac{dn(z,>M)}{d\log M}$.

In figures 5.6 and 5.5, we plot and compare $\frac{dn(z,>M)}{d\log M}$ and $n(>M)$ of the halos created from wakes with the predictions based on the Press-Schechter formalism as found in Reed et al. [47]. We use the string parameters

$$G\mu = 1.5 \times 10^{-7},\ \tilde{N} = 10,\ v_s = 1/2 \text{ and } \gamma = 1. \tag{5.19}$$

Note that the "wiggles" in the plots of $n(>M)$ are just an artefact of our interpolation.

Using the current bound on $G\mu$ in equation 5.19, we see from the figures 5.6 and 5.5 that structures formed from primordial fluctuations start to dominate before redshift $z = 20$. Even if the wake halos make up a possibly noticeable fraction of the total halos in the small mass region at any redshift, objects of these masses are hard to detect. Therefore, mapping the mass function in that range is far from currently possible.

Nevertheless, if we could manage to detect the halos, this mass function statistic misses the crucial point that the halos from the same string wake will have a strong position space correlation between them. They will have similar masses and lie in the same plane. This will aid a search for such cosmic string signals. We will investigate detecting this possible signature in section 6.

At this point our whole discussion has been assuming no interactions between wakes and primordial fluctuations. Such interaction will have minimal impact on the formation of the very large structures ($\geq 10^{10} - 10^{11}\mathrm{M}_{\odot}$) since these are formed by collapse of a length scale much larger than can be affected by a wake. However a large primordial density fluctuation can distort and even destroy the fragile correlation between the wake's halos.

We give a rough estimate of the number of surviving wakes by determining the

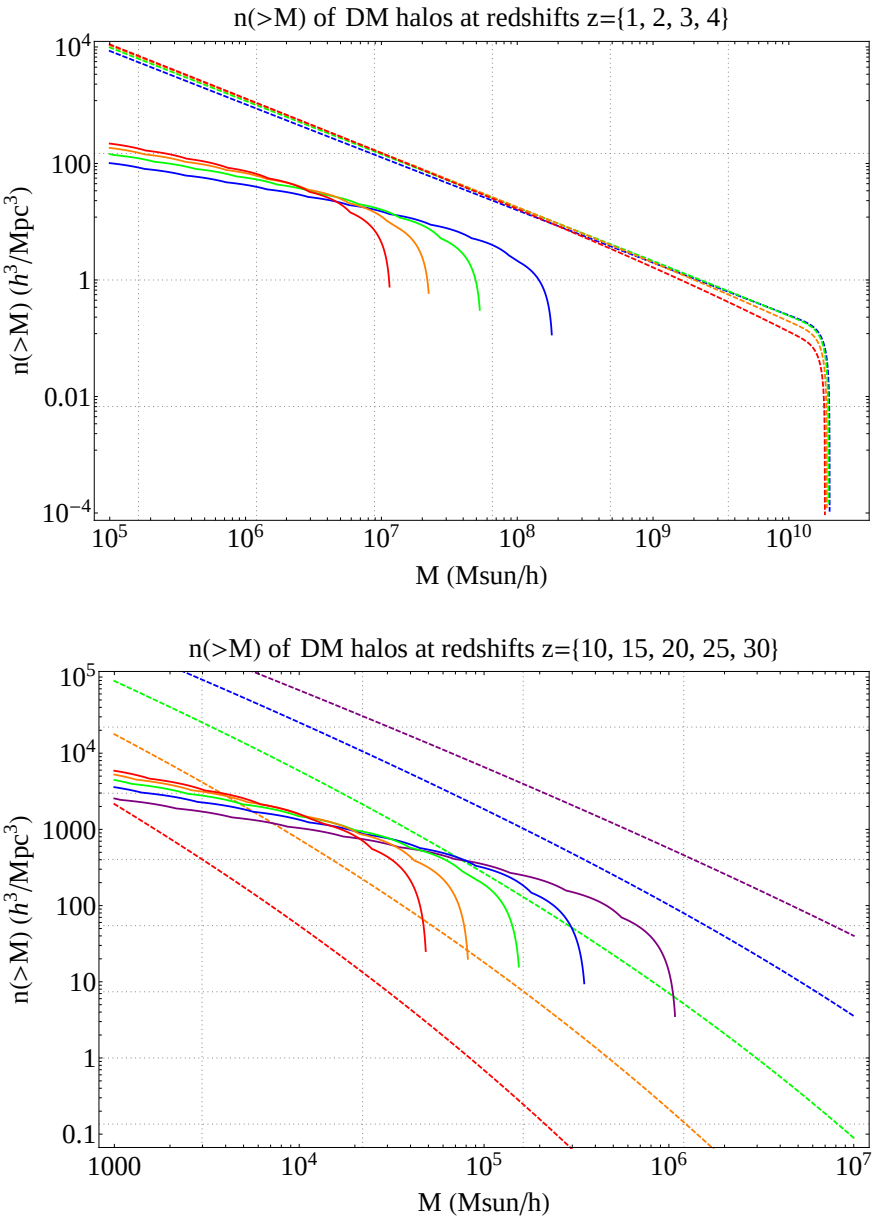

Figure 5.5: $n(>M)$ of dark matter halos for a string network with $G\mu = 1.5 \times 10^{-7}$ (solid) and the Reed et al. [47] predictions (dashed) at different redshifts. The colors with largest wavelength corresponds to the largest redshifts.

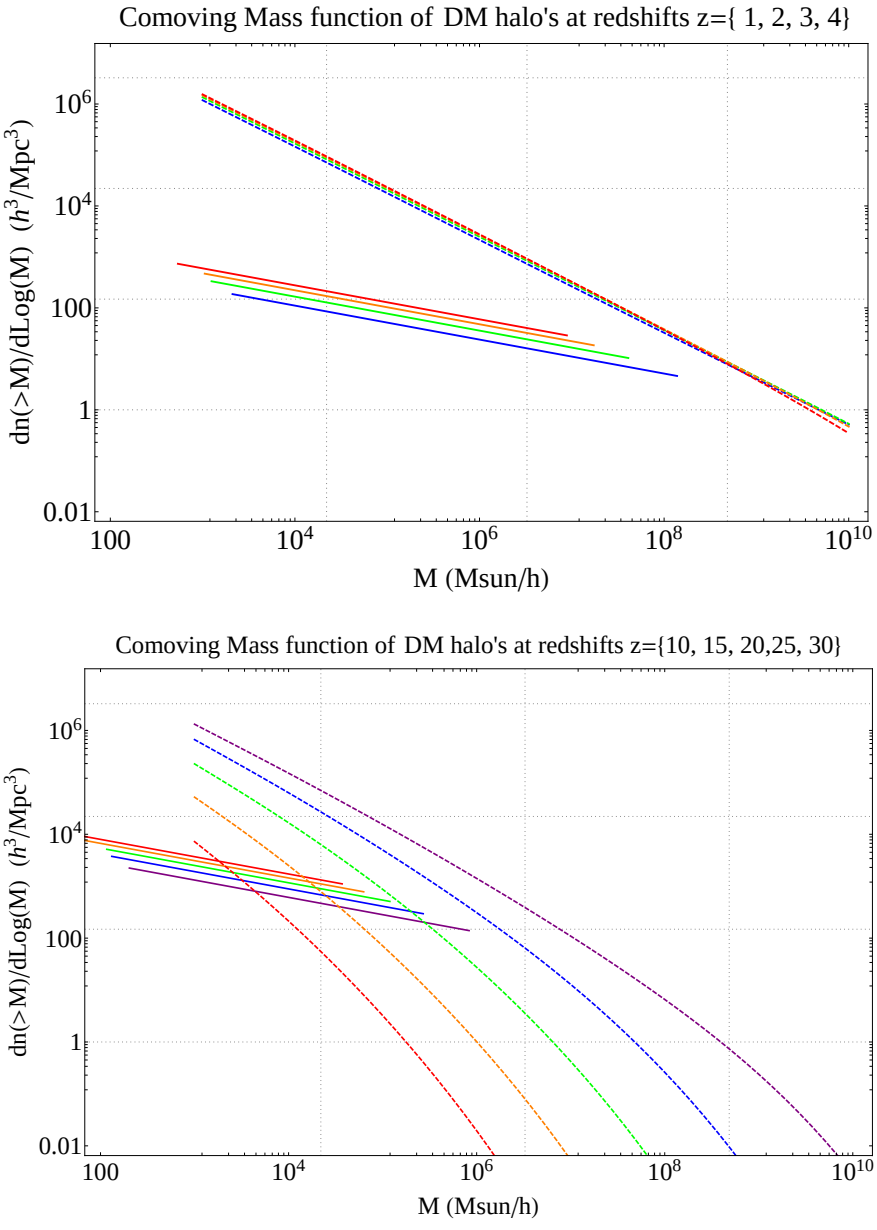

Figure 5.6: Mass function of dark matter halos for a string network with $G\mu = 1.5\times10^{-7}$ (solid) and the Reed et al.[47] predictions (dashed) at different redshifts. The colors with largest wavelength corresponds to the largest redshifts.

fraction of space that are voids with no large halos. The fraction of space that collapsed in Gaussian noise-induced halos of mass greater than M is given by [41],

$$F(>M,z) = 2\int_{\delta_{crit}(z)}^{\infty} \mathrm{d}\delta \frac{1}{\sqrt{2\pi}\sigma(M)} \exp\Big(-\frac{\delta^2}{2\sigma(M)^2}\Big)$$
$$= \mathrm{Erfc}\Big(\frac{\delta_{crit}(z)}{\sqrt{2}\sigma(M)}\Big). \tag{5.20}$$

Here, $\delta_{crit} = 1.686(1+z)$ and $\sigma(M)$ is the rms density fluctuation on a comoving length scale $R = (3M/4\pi\rho_0(0))^{1/3}$ which, as we've seen, depends on the power spectrum of matter. Figure 5.7 shows $F(>M_w, z)$ for three different values of $G\mu$. Here $M_w(z, G\mu)$ is the maximum mass of wake halos. We also plot $F(>10^3 M_\odot/h, z)$ which was the smallest mass that was resolved in the simulation by Reed et al. [47]. If F is close to 1, then most of the matter was accreted onto large Gaussian noise-induced halos, and therefore these large halos wiped out any geometrical structures and spatial correlations that wake halos could possess. As the figure shows, the larger the redshift is, the less will be the washout of string-induced structures by the Gaussian noise.

Before moving our discussion to the search of observational signals in the large scale structures, we briefly mention the problems with another observational window. Studies using observations of γ-rays flux allow for constraints on the populations of ultracompact minihalos (UCMH) [69]. The UCMHs are created in the early universe ($z \gtrsim 100$) as isolated objects insuring that their formation is well approximated by a radial infall picture. We expect structures from string wakes to dominate over the ones formed by the primordial fluctuations at high redshift. This suggests that the contribution to the population of UCMH friom wakes could impose constraints on $G\mu$. Following this idea, we hit a wall when trying to determine the density profile of the UCMHs formed in the wakes. The bulk motion of the matter inside the wake oscillate around the center. This will cause heavy tidal forces on the growing perturbations and hence mess up the nice spherical accretion needed

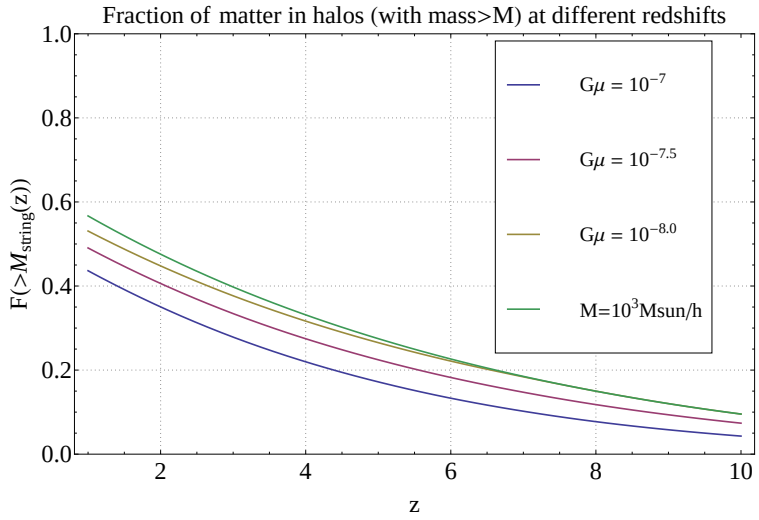

Figure 5.7: Fraction of matter in halos of mass greater than wakes can create. We plot the curves for multiple values of $G\mu$ and one of a mass of $10^3 M_\odot$ for reference. These were computed with the program supplied in [47].

to produce reliable density profiles. Therefore it is unlikely that structures formed in wakes can be used to give accurate predictions as in [69]. The situation will be different when considering string loops since they accrete matter because of their Newtonian potential. That situation was studied in [36].

6

String Wakes in the Large Scale Structure

6.1 Gravitational Lensing

Very little star formation is expected in wake halos and so we must find ways that does not rely on optical methods to detect them. Since they are still massive, could gravitational lensing work (for reviews on gravitational lensing see [72],[73])? We would expect the wakes and their substructure to create specific signatures from their lensing of background sources.

Consider a mass distribution (the lens) and a source located away from us at an angular distance of d_l, d_s respectively. If the mass distribution is small in extent compared to d_l, d_s, then we can define the deflection angle α. This measures how much bendingl the geodesics of light will suffer as they propagate past the lens (see figure 6.1). This quantity is given by [73],

$$\vec{\alpha}(\vec{\xi}) = \frac{4G}{c^2}\int_V \mathrm{d}\xi_1'\mathrm{d}\xi_2'\mathrm{d}\mathrm{r}_3'\rho(\xi_1',\xi_2',\mathrm{r}_3')\frac{\vec{\xi}-\vec{\xi'}}{|\vec{\xi}-\vec{\xi'}|^2}, \tag{6.1}$$

where r_3 is the radial distance, the ξ's are the perpendicular coordinates and ρ is the density of matter. The true position of the source in the sky $\vec{\beta}$ can be related to the observed one $\vec{\theta} = \vec{\xi}/d_l$ through the lens equation,

$$\vec{\beta} = \vec{\theta} - \frac{d_s - d_l}{d_s}\vec{\alpha}(d_l\vec{\theta})), \tag{6.2}$$

The term weak lensing is used if this equation can be inverted to obtain a one-to-one correspondence between θ and β while strong lensing refers to the cases in which multiple images are produced (i.e. multiple θ relating to one β). The distortion matrix $\mathcal{A}(\vec{\theta}) = \partial\vec{\beta}/\partial\vec{\theta}$ encodes the information about the distortion and magnification of images.

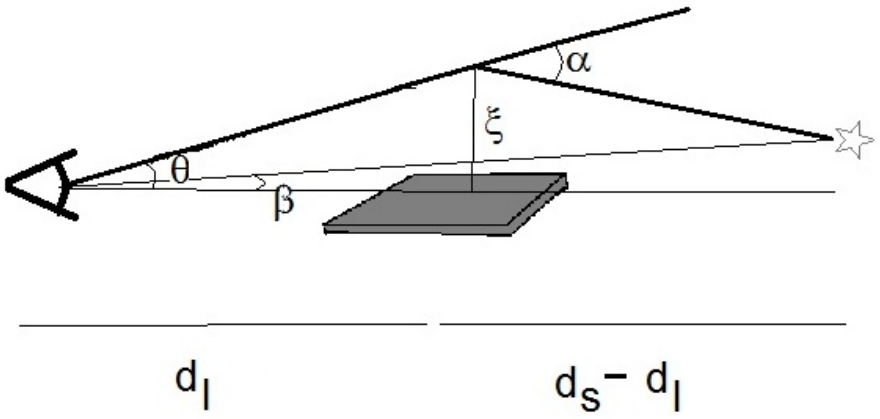

Figure 6.1: Strong lensing of a background source due to a string wake.

6.1.1 Weak Lensing by the wake's halos

Recent advances in weak gravitational lensing ([74], [75]) allows detection of very small dark matter halos in the mass range of $10^6 M_\odot - 10^8 M_\odot$. They do so by looking at an unexpected distortion in one of the many images in strongly lensed systems and can then infer the mass of the object causing the anomaly. Any clumps of matter intersecting the path of the light rays will cause lensing and hence distortion; it is expected that around 90% of the halos detected with this method are not part of the lens [76]. Since the dark matter halos created from cosmic string wakes will have a very strong correlation in position space, we can hope that a wake intersecting the geodesics of the source's light rays would cause image distortions that would allow us to detect such spatial correlations.

To determine the probability that a wake intersects such a geodesic we focus on the ones formed at t_{eq} since these are the most numerous and will possess the most massive halos. The number of string wakes intersecting the hypersurface S^2 at redshift z was calculated in [71] and is given by,

$$N_{S^2}(z) = 4\pi\tilde{n}_{wake}(z_{eq})(1+z)^3 v_s R_{eq}^2 H_{eq}^{-1}\Big(\frac{\sqrt{\pi\gamma v_s\gamma_s}}{3v_s\cos(\theta_s)}\Big), \tag{6.3}$$

where $\cos(\theta_s) = \frac{1}{\sqrt{2}}$ is the average orientation of string wakes, $R_{eq} = 3t_{eq}^{2/3}(t_0^{1/3} - t_z^{1/3})$ is the physical radius of the hypersurface S^2 at t_{eq}, H_{eq} is the Hubble parameter at that time and $\tilde{n}_{wake}(z_{eq})$ is the comoving number density of wakes given by equation 5.16.

The probability that a wake located at redshift z does **not** intersect along our line-of-sight a lensed image that spans an angle θ in the sky is,

$$P(z) = \Big(\frac{A_{S^2} - A_\theta}{A_{S^2}}\Big)^{N_{S^2}(z)} = \Big(\frac{1}{2} + \frac{1}{2}\cos(\theta/2)\Big)^{N_{S^2}(z)}, \tag{6.4}$$

with A_θ being the area in the sky taken by the lensed image, and $A_{S^2} = 4\pi$ the area covered by the whole sky.

In redshift space, the average thickness of the wakes is,

$$l = \frac{\gamma + \gamma_s v_s}{2\sqrt{2}}\Big(\frac{z+1}{z_{eq}+1}\Big)^{1/2}. \tag{6.5}$$

Therefore, if we discretize redshift space in bins of size $\Delta z = a(t_0)\big(\frac{1}{a(t(z))} - \frac{1}{a(t(z)+l)}\big)$ so that $z_1 = 0,\ z_2 = z_1 + \Delta z(z_1),\ ...,\ z_m = z_{m-1} + \Delta z(z_{m-1})$, we are assured that wakes cannot intersect more than one hypersurface, and hence the probabilities in eq. 6.4 are independent for different z_i. This allows us to get a good estimate on the probability that a wake intersects our line-of-sight with a lensed image,

$$P = 1 - \prod_{z_i=0}^{z_m<z_{lens}} P(z_i). \tag{6.6}$$

Using the parameters of 5.19 with a lens of size $\theta = 1$ arcsec at $z_{lens} = 2$, we find $P \approx 3\times10^{-6}$. This is a very small number considering that there are 572 lenses

catalogued in the Master Lens database [77] as of March 2013. The lens number is expected to increase drastically in the next few years but considering that we would require 300000 lens to statistically constrain strings we don't expect this method to be viable in the foreseeable future. The situation does not get better if we include wakes formed at later times, the probability of intersection stays the same order of magnitude.

6.1.2 Strong Lensing by the wake itself

A wake formed at t_{eq} with parameters in 5.19 will have grown to a mass of about $10^{14}\mathrm{M}_{\odot}$ at $z = 0$. In the case of a spherical lens, this is enough mass to create lensed images with Einstein radius of 0.3 arcsec. In the case of a wake, its orientation is important. Consider an observer who looks through a wake on its side as in figure 6.1. If the wake is located at a redshift z_l it will have dimension $L \times L \times w$ with $L(z_l) = \frac{1}{2}c(\gamma t_{eq} + v_s\gamma_s t_{eq})\frac{a(z_l)}{a(z_{eq})}$ being the average length of its sides. The density of matter ρ in equation 6.1 will only be non-zero inside the wake and take a value of $\rho(z_l) = \frac{4}{6\pi G t_0^2}(z_l+1)^3$. Assuming $w(z_l) \ll \xi_1 \ll L(z_l)$ we can treat the wake as an infinite line in the ξ_2' direction passing through $(r_3', \xi_1') = (d_l, 0)$ and with mass per unit length obtained by performing the $\mathrm{d}\xi_1'\mathrm{d}r_3'$ integrals of equation 6.1. With these simplification we have that $\alpha_2 = 0$ and,

$$\alpha_1(\vec{\xi}) = \frac{4G}{c^2}\rho(z_l)L(z_l)w(z_l)\int_{-\infty}^{\infty}\mathrm{d}\xi_2'\frac{\xi_1}{\xi_1^2 + (\xi_2 - \xi_2')^2} \tag{6.7}$$

$$= \frac{4G}{c^2}\rho(z_l)L(z_l)w(z_l)\pi\mathrm{sgn}(\xi_1) \tag{6.8}$$

$$= \frac{32G\mu v_s\gamma_s}{5}(\gamma + v_s\gamma_s)\pi\mathrm{sgn}(\xi_1) = C(z_l)\mathrm{sgn}(\xi_1). \tag{6.9}$$

This $\vec{\alpha}$ gives us two solutions to the lens equation 6.2,

$$\beta_1 = \theta_1 - \frac{d_s - d_l}{d_s}C(z_l)\mathrm{sgn}(\theta_1),\ \beta_2 = \theta_2. \tag{6.10}$$

To lowest order, the matrix $\mathcal{A}(\vec{\theta})$ of this solution is the identity and therefore there is no magnification or distortion in the images. This is the same lensing effect

that the conical geometry around a string would produce, namely two images with no magnification or distortion. For example, using the parameters of equations 5.19, a wake at redshift 1 lensing a source at redshift 2 would create two images separated by ~ 0.2 arcsec in the sky. Note how $L \sim 50\text{Mpc} \gg \xi_1 \sim 1.6\text{Mpc} \gg w \sim 0.15\text{Mpc}$ justifies our original simplification. In order to have enough mass along the integrated line of sight to get strong lensing we require that the background source lies, with us, very close to the plane delimited by a wake. This makes the signal too rare to be useful to statistically constrain string parameters. However, if one were lucky, assuming the images do not overlap, which could happen for extended source and a small $G\mu$ or if we are not in the proximity of the wake's plane, a lensed source would appear as two images with no magnification or distortion. In such a case one could hope to find other similarily lensed objects along some line in the sky.

6.2 Topological Signature of wakes and Minkowski Functionals

As previously discussed, halos from wakes should have strong position space correlations amongst themselves. If we could some day detect halos in the relevant (small) mass range, it would be interesting to see how observable this correlation would be compared to the background. In order to do this we employ a tool - namely Minkowski functionals - already used in cosmology (see [78] for examples) and that allows to characterize the geometric properties of shapes. The large scale structures seeded by wakes will have a different shape than the ones seeded from Gaussian random fluctuations since the former should coherently create structures along planes. However we will see that non-linear growth of the background perturbations are able to mimic the wakes signal, making it hard to resolve. We first give a brief overview of Minkowski functionals before applying it to our problem while directing the reader to [79] for additional details.

6.2.1 Minkowski Functionals

We would like to find a set of operators that allows us to characterize different shapes. Geometric characteristics of a set should satisfy certain requirements which our operator V will also follow. Consider a convex body $\mathcal{E}$, then we impose the following three properties that V acting on $\mathcal{E}$ must obey,

- Motion Invariance

  Changing the position of our manifold $\mathcal{E}$ by some action of a group $\mathcal{G}$ should not affect the value of the functional. Namely, $\forall g \in \mathcal{G}$

  $$V(\mathcal{E}) = V(g\mathcal{E}). \tag{6.11}$$

- Additivity

  If we have two sets $\mathcal{E}$ and $\mathcal{D}$, their geometric properties should add and hence the functional should satisfy,

  $$V(\mathcal{E} \cup \mathcal{D}) = V(\mathcal{E}) + V(\mathcal{D}) - V(\mathcal{E} \cap \mathcal{D}). \tag{6.12}$$

- Conditional Continuity

  Finally the functionals of convex approximations $\mathcal{E}_i$ to a convex set $\mathcal{E}$ should converge. Namely,

  $$V(\mathcal{E}_i) \to V(\mathcal{E}), \text{ as } \mathcal{E}_i \to \mathcal{E} \text{ for } i \in I. \tag{6.13}$$

The possible functionals obeying the above are very restricted, a fact captured by Hadwiger's theorem [80]. The theorem states that for a convex body in d dimensional space, there exists only $d+1$ linearly independent functionals M_i, $i \in \{1, ...d+1\}$ satisfying the above three conditions. In three (spatial) dimensions, these can be chosen to be the *fractional volume* V, the *surface area* A, the *mean curvature* H and the

Euler characteristic χ of our set $\mathcal{E}$. The details involved in computing these can be found, along with information about programs already written to do the job, in [79].

How do we use the above data to pick out signals from the large scale structure? Consider an arbitrary density $\rho(x)$ in a box of length L. Define ρ_{avg} to be the average value and σ to be the standard deviation. Now if we remove all points of space with $\rho(x) < \rho_{avg} + v\sigma$ a shape is formed from the remainder. The previous operation can be thought of as setting

$$\rho(x) = 0, \text{ if } \rho(x) < \rho_{avg} + cv \tag{6.14}$$

$$\rho(x) = 1, \text{ if } \rho(x) \geq \rho_{avg} + cv, \tag{6.15}$$

and obtaining the resulting shape defined by the x's that have $\rho(x) = 1$. This is called the excursion set and we can evaluate its corresponding Minkowski functionals. The functionals will depend on the threshold v and hence allow for plots $M_i(v)$ that will look quite different for various density distributions. For instance, imagine how the fractional volume $V = M_1$ changes for a distribution with a nearly homogeneous density profile; it will look similar to a step function since for $v < 0$ all our points are included so we will have $M_i(v) \approx 1$ and then there will be a sharp decrease so that $M_i(v) = 0$ for $v > 0$. For random Gaussian fluctuations, the curve will run from 1 to 0 much more smoothly as we increase v.

Our goal will be to compare the Minkowski functionals of a *density of halos* made from cosmic strings and primordial fluctuation against a distribution made only from primordial fluctuations. We should be able to see a difference if the wakes create many planar-like structures since they will appear as a very distinct shape in the functional curve. To generate the wake halos distributions, we laid down wakes at random positions and orientation in a box of size $(50Mpc)^3$ then fragmented them into halos according to the results we previously discussed. Generating maps of the background is much trickier. We are interesting in a redshift where the initial

perturbations - being a Gaussian random field - had time to evolve into non-linear structures. To obtain different realizations of the final structure, we must resort to N-body simulations which can resolve halos of mass below $10^7 M_\odot$. These are computationally expensive and complex to perform. To simplify our life we use the data from the Millennium-II simulation [81], a N-body simulation done in a box of size $(100Mpc)^3$ which can resolve halos down to $10^6 M_\odot$. This only allowed us to obtain 8 independent maps of background structure (each corner of the simulation). We computed the Minkowski functionals of those maps then averaged them. We did the computation a second time, but now we added the halos from the string wakes on top of the background. We then compared the averaged Minkowski functionals of the two model (string+background) and (background). One thing to note is that the background between the two model will be **100**% correlated, we will come back to this point in a moment.

In figures 6.2.1 we show the averaged Minkowski functionals of the *background* in blue, along with the error bars, compared to the average Minkowski functionals of the *background + string wakes* in black. The different is noticeable but expected. Because the backgrounds are so correlated, any additional change to the maps (like adding a set of wake halos) will change the geometry of the excursion set.

Just by eye, this looks like a distinguishable signal. However we did not take into account how large primordial perturbations would affect the wake's geometry. We gave a quick estimate that roughly $\sim 50\%$ of the wakes will be destroyed (this can be seen in figure 5.7). We try to capture this dynamics by removing randomly 50% of the wake network and repeating the Minkowski functional calculation. The result is shown in figure 6.2.1 and it is already a lot harder to see the a difference. Figure 6.2.1 shows the same result but with error bars on both curves, rendering them nearly indistinguishable. The reason the background and the combined background + wake curves look similar is because primordial fluctuations also tends to

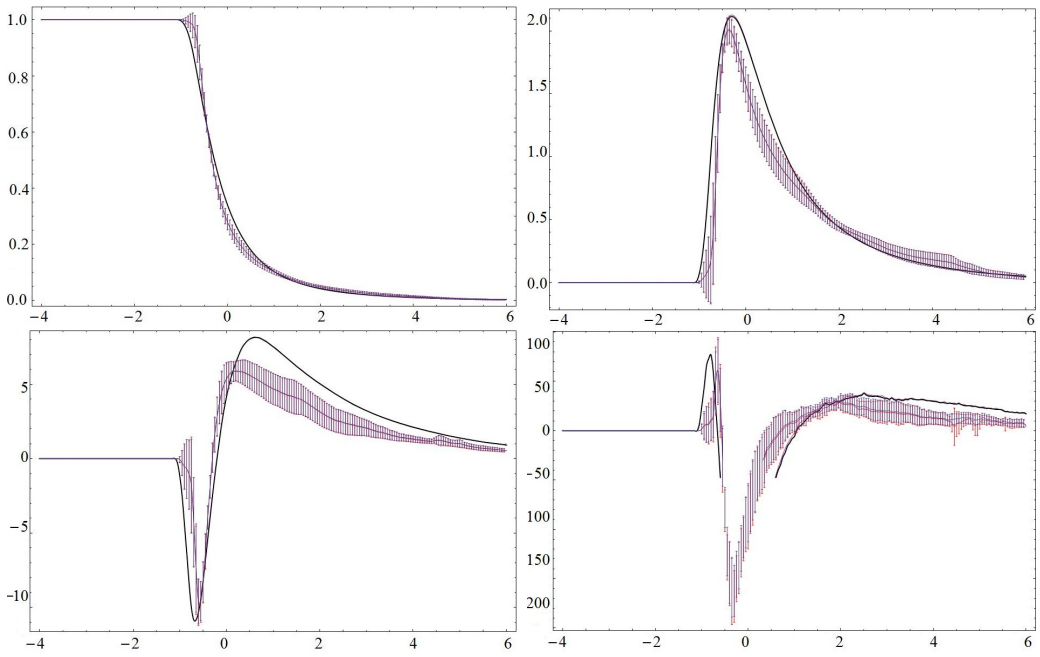

Figure 6.2: Comparison of the average Minkowski functionals for excursion sets defined by v between background structures (blue) and background+wake structures (black). The Minkowski functionals are M_1 (top left), M_2 (top right), M_3 (bottom left) and M_4 (bottom right).

form sheet-like structures as they agglomerate into dense clumps, an effect called the Zel'dolvich pancake. Hence even with no string wakes, there will still be sheet-like structures present. Of course the string wakes will have specific dimensions whereas the Zel'dovich pancakes would have more random properties. With much more background maps and a finer resolution one could possibly detect the wake signals using Minkowski functionals. The lack of background maps (only 8) renders our current analysis very fragile but we did not carry the work further since realistically mapping the density of matter with the accuracy needed is far from currently possible in the foreseeable future.

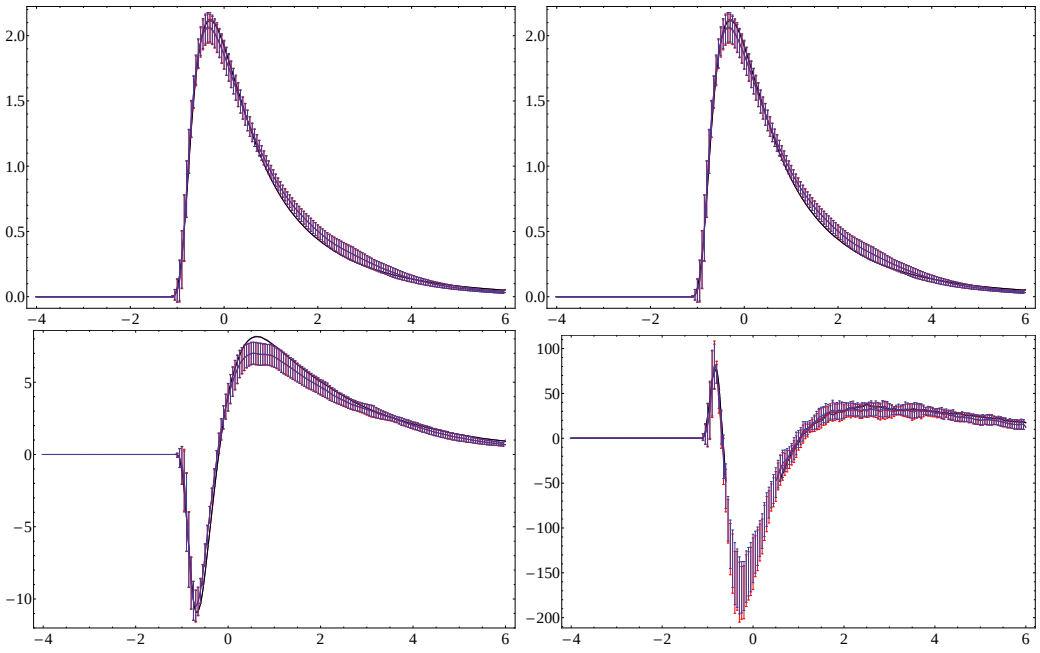

Figure 6.3: Comparison of the average Minkowski functionals for excursion sets defined by v between background structures (blue) and background+wake structures (black). However this time we took into account the backreaction of the background on the wake structure. The Minkowski functionals are M_1 (top left), M_2 (top right), M_3 (bottom left) and M_4 (bottom right).

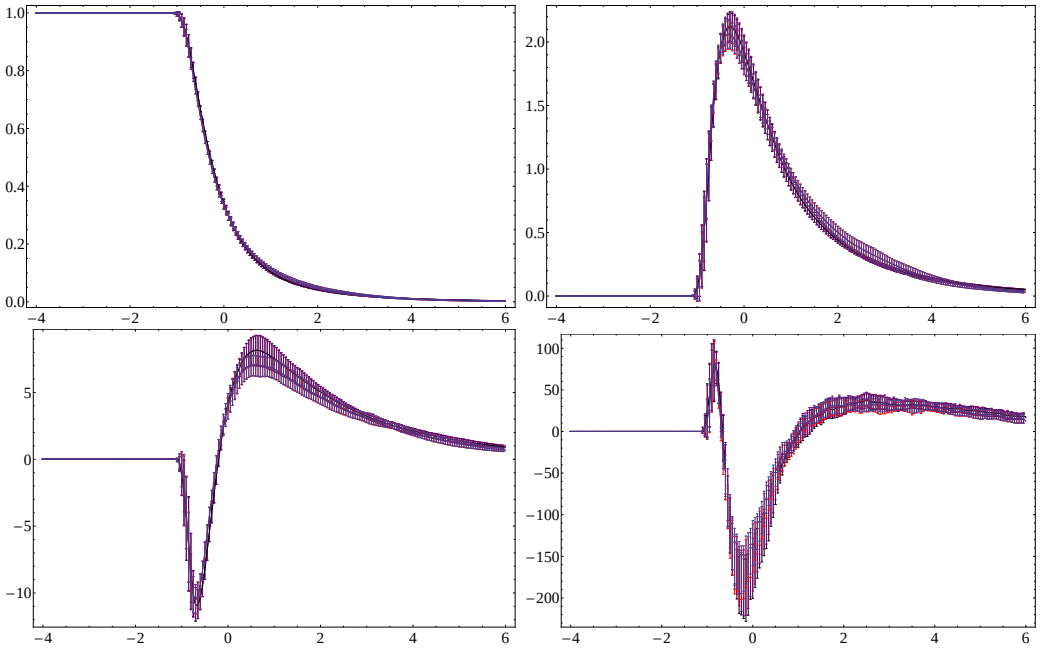

Figure 6.4: Same situation as in figure 6.2.1 but this time with error bars on both curves.

7

Conclusion

In this thesis we first reviewed the theory of structure formation and cosmic strings. Strings come in two different shapes, namely long strings and string loops, their population distributions were qualitatively different but both evolved following a scaling solution proportional to the horizon size. The two shapes also have different effects on the surrounding matter: loops possess a Newtonian potential that directly causes matter to be attracted while long "infinite" strings have no local gravitational potential but generate wakes of non-linear density perturbations as they move through matter. Structure formation from string loops was previously studied in [32], where it was found that string loops with mass $G\mu \sim 10^{-7}$ (the current constraint [17]) would produce halos with significant star formation at early times and have an impact on the period of reionization. This prompted us to study the structure formed from the other part of the network, namely the long strings. We showed that observational signals in the large scale structure from string wakes are challenging to detect [1]. To be more precise, we have shown that string wakes dominate the nonlinear structures in the universe at sufficiently high redshifts, and at lower redshifts they may be identifiable from the background because of the distinct spatial correlations which they induce. However we argued afterwards that the string-induced halos are typically too cold to induce star formation and observe them through optical telescopes, and too light and rare to be detected by gravitational lensing techniques. Moreover the non-linear background is able to mimic the

planar correlations between wake halos which makes these challenging to extract. One promising window - studied in other works [62, 82, 83, 84, 85] - is via 21cm redshift surveys.

Bibliography

[1] F. Duplessis, R. Brandenberger, *Note on Structure Formation from Cosmic String Wakes*, 2013, [arXiv:1302.3467]

[2] R. Jeannerot, "A Supersymmetric SO(10) Model with Inflation and Cosmic Strings," Phys. Rev. D **53**, 5426 (1996) [arXiv:hep-ph/9509365];
R. Jeannerot, J. Rocher and M. Sakellariadou, "How generic is cosmic string formation in SUSY GUTs," Phys. Rev. D **68**, 103514 (2003) [arXiv:hep-ph/0308134].

[3] S. Sarangi and S. H. H. Tye, "Cosmic string production towards the end of brane inflation," Phys. Lett. B **536**, 185 (2002) [arXiv:hep-th/0204074];
E. J. Copeland, R. C. Myers and J. Polchinski, "Cosmic F- and D-strings," JHEP **0406**, 013 (2004) [arXiv:hep-th/0312067].

[4] R. H. Brandenberger and C. Vafa, "Superstrings in the Early Universe," Nucl. Phys. B **316**, 391 (1989);
A. Nayeri, R. H. Brandenberger and C. Vafa, "Producing a scale-invariant spectrum of perturbations in a Hagedorn phase of string cosmology," Phys. Rev. Lett. **97**, 021302 (2006) [arXiv:hep-th/0511140];
R. H. Brandenberger, A. Nayeri, S. P. Patil and C. Vafa, "String gas cosmology and structure formation," Int. J. Mod. Phys. A **22**, 3621 (2007) [hep-th/0608121];
R. H. Brandenberger, "String Gas Cosmology," arXiv:0808.0746 [hep-th].

[5] T. W. B. Kibble, "Topology of Cosmic Domains and Strings," J. Phys. A **9**, 1387 (1976);

T. W. B. Kibble, "Some Implications of a Cosmological Phase Transition," Phys. Rept. **67**, 183 (1980);
T. W. B. Kibble, "Phase Transitions In The Early Universe," Acta Phys. Polon. B **13**, 723 (1982).

[6] Y. B. Zeldovich, "Cosmological fluctuations produced near a singularity," Mon. Not. Roy. Astron. Soc. **192**, 663 (1980);
A. Vilenkin, "Cosmological Density Fluctuations Produced By Vacuum Strings," Phys. Rev. Lett. **46**, 1169 (1981) [Erratum-ibid. **46**, 1496 (1981)];
N. Turok and R. H. Brandenberger, "Cosmic Strings And The Formation Of Galaxies And Clusters Of Galaxies," Phys. Rev. D **33**, 2175 (1986);
H. Sato, "Galaxy Formation by Cosmic Strings," Prog. Theor. Phys. **75**, 1342 (1986);
A. Stebbins, "Cosmic Strings and Cold Matter", Ap. J. (Lett.) **303**, L21 (1986).
N. Deruelle, D. Langlois, J.P. Uzan, "Cosmological Perturbations seeded by Topological Defects: Setting the Initial Conditions", Phys. Rev. D56 (1997) 7608, [arXiv:gr-qc/9707035]

[7] J. Magueijo, A. Albrecht, D. Coulson and P. Ferreira, "Doppler peaks from active perturbations," Phys. Rev. Lett. **76**, 2617 (1996) [arXiv:astro-ph/9511042];
U. L. Pen, U. Seljak and N. Turok, "Power spectra in global defect theories of cosmic structure formation," Phys. Rev. Lett. **79**, 1611 (1997) [arXiv:astro-ph/9704165];
L. Perivolaropoulos, "Spectral Analysis Of Microwave Background Perturbations Induced By Cosmic Strings," Astrophys. J. **451**, 429 (1995) [arXiv:astro-ph/9402024].

[8] P. D. Mauskopf *et al.* [Boomerang Collaboration], "Measurement of a Peak in the Cosmic Microwave Background Power Spectrum from the North Ameri-

can test flight of BOOMERANG," Astrophys. J. **536**, L59 (2000) [arXiv:astro-ph/9911444].

[9] L. Perivolaropoulos, "COBE versus cosmic strings: An Analytical model," Phys. Lett. B **298**, 305 (1993) [arXiv:hep-ph/9208247];
L. Perivolaropoulos, "Statistics of microwave fluctuations induced by topological defects," Phys. Rev. D **48**, 1530 (1993) [arXiv:hep-ph/9212228].
A. Riazuelo, N. Deruelle, P. Peter, "Topological Defects and CMB anisotropies : Are the predictions reliable ?", Phys. Rev. D61. (2000) 123504, [astro-ph/9910290]

[10] R. H. Brandenberger, "Topological defects and structure formation," Int. J. Mod. Phys. A **9**, 2117 (1994) [arXiv:astro-ph/9310041].

[11] J. H. Traschen, N. Turok and R. H. Brandenberger, "Microwave Anisotropies from Cosmic Strings," Phys. Rev. D **34**, 919 (1986);
R. H. Brandenberger and N. Turok, "Fluctuations From Cosmic Strings And The Microwave Background," Phys. Rev. D **33**, 2182 (1986).

[12] R. H. Brandenberger, R. J. Danos, O. F. Hernandez and G. P. Holder, "The 21 cm Signature of Cosmic String Wakes," JCAP **1012**, 028 (2010) [arXiv:1006.2514 [astro-ph.CO]].

[13] R. J. Danos, R. H. Brandenberger and G. Holder, "A Signature of Cosmic Strings Wakes in the CMB Polarization," Phys. Rev. D **82**, 023513 (2010) [arXiv:1003.0905 [astro-ph.CO]].

[14] L. Pogosian & M. Wyman, *B-modes from Cosmic Strings,* Phys. Rev. D 77, 083509 (2008) [arXiv: 0711.0747].
A. Avgoustidis et al., *Constraints on the fundamental string coupling from B-mode experiments,* Phys. Rev. Lett. 107, 121301 (2011) [arXiv:1105.6198].

[15] J. E. Ruhl *et al.* [The SPT Collaboration], "The South Pole Telescope," Proc. SPIE Int. Soc. Opt. Eng. **5498**, 11 (2004) [arXiv:astro-ph/0411122];
J. E. Carlstrom *et al.*, "The 10 Meter South Pole Telescope," Publ. Astron. Soc. Pac. **123**, 568 (2011) [arXiv:0907.4445 [astro-ph.IM]].

[16] D. Larson, J. Dunkley, G. Hinshaw, E. Komatsu, M. R. Nolta, C. L. Bennett, B. Gold and M. Halpern *et al.*, "Seven-Year Wilkinson Microwave Anisotropy Probe (WMAP) Observations: Power Spectra and WMAP-Derived Parameters," Astrophys. J. Suppl. **192**, 16 (2011) [arXiv:1001.4635 [astro-ph.CO]].

[17] C. Dvorkin, M. Wyman and W. Hu, "Cosmic String constraints from WMAP and the South Pole Telescope," Phys. Rev. D **84**, 123519 (2011) [arXiv:1109.4947 [astro-ph.CO]].

[18] L. Pogosian, S. H. H. Tye, I. Wasserman and M. Wyman, "Observational constraints on cosmic string production during brane inflation," Phys. Rev. D **68**, 023506 (2003) [Erratum-ibid. D **73**, 089904 (2006)] [arXiv:hep-th/0304188];
M. Wyman, L. Pogosian and I. Wasserman, "Bounds on cosmic strings from WMAP and SDSS," Phys. Rev. D **72**, 023513 (2005) [Erratum-ibid. D **73**, 089905 (2006)] [arXiv:astro-ph/0503364];
A. A. Fraisse, "Limits on Defects Formation and Hybrid Inflationary Models with Three-Year WMAP Observations," JCAP **0703**, 008 (2007) [arXiv:astro-ph/0603589];
U. Seljak, A. Slosar and P. McDonald, "Cosmological parameters from combining the Lyman-alpha forest with CMB, galaxy clustering and SN constraints," JCAP **0610**, 014 (2006) [arXiv:astro-ph/0604335];
R. A. Battye, B. Garbrecht and A. Moss, "Constraints on supersymmetric models of hybrid inflation," JCAP **0609**, 007 (2006) [arXiv:astro-ph/0607339];
R. A. Battye, B. Garbrecht, A. Moss and H. Stoica, "Constraints on Brane Inflation and Cosmic Strings," JCAP **0801**, 020 (2008) [arXiv:0710.1541 [astro-ph]];

N. Bevis, M. Hindmarsh, M. Kunz and J. Urrestilla, "CMB power spectrum contribution from cosmic strings using field-evolution simulations of the Abelian Higgs model," Phys. Rev. D **75**, 065015 (2007) [arXiv:astro-ph/0605018];
N. Bevis, M. Hindmarsh, M. Kunz and J. Urrestilla, "Fitting CMB data with cosmic strings and inflation," Phys. Rev. Lett. **100**, 021301 (2008) [astro-ph/0702223 [ASTRO-PH]];
R. Battye and A. Moss, "Updated constraints on the cosmic string tension," Phys. Rev. D **82**, 023521 (2010) [arXiv:1005.0479 [astro-ph.CO]].

[19] J. Urrestilla, N. Bevis, M. Hindmarsh, and M. Kunz, "Cosmic string parameter constraints and model analysis using small scale Cosmic Microwave Background data," JCAP **1112**, 021 (2011) [arXiv:1108.2730 [astro-ph.CO]].

[20] A. Kosowsky [the ACT Collaboration], "The Atacama Cosmology Telescope Project: A Progress Report," New Astron. Rev. **50**, 969 (2006) [arXiv:astro-ph/0608549].

[21] S. Amsel, J. Berger and R. H. Brandenberger, "Detecting Cosmic Strings in the CMB with the Canny Algorithm," JCAP **0804**, 015 (2008) [arXiv:0709.0982 [astro-ph]];
A. Stewart and R. Brandenberger, "Edge Detection, Cosmic Strings and the South Pole Telescope," JCAP **0902**, 009 (2009) [arXiv:0809.0865 [astro-ph]];
R. J. Danos and R. H. Brandenberger, "Canny Algorithm, Cosmic Strings and the Cosmic Microwave Background," Int. J. Mod. Phys. D **19**, 183 (2010) [arXiv:0811.2004 [astro-ph]].

[22] M. S. Movahed, B. Javanmardi and R. K. Sheth, "Peak-peak correlations in the cosmic background radiation from cosmic strings," arXiv:1212.0964 [astro-ph.CO].

[23] V. Berezinsky, K. D. Olum, E. Sabancilar and A. Vilenkin, "UHE neutrinos from superconducting cosmic strings," Phys. Rev. D **80**, 023014 (2009) [arXiv:0901.0527 [astro-ph.HE]];
C. Lunardini and E. Sabancilar, "Cosmic Strings as Emitters of Extremely High Energy Neutrinos," Phys. Rev. D **86**, 085008 (2012) [arXiv:1206.2924 [astro-ph.CO]].

[24] Y. -F. Cai, E. Sabancilar, D. A. Steer and T. Vachaspati, "Radio Broadcasts from Superconducting Strings," Phys. Rev. D **86**, 043521 (2012) [arXiv:1205.3170 [astro-ph.CO]];
T. Vachaspati, "Cosmic Sparks from Superconducting Strings," Phys. Rev. Lett. **101**, 141301 (2008) [arXiv:0802.0711 [astro-ph]];
Y. -F. Cai, E. Sabancilar and T. Vachaspati, "Radio bursts from superconducting strings," Phys. Rev. D **85**, 023530 (2012) [arXiv:1110.1631 [astro-ph.CO]];
V. Berezinsky, B. Hnatyk and A. Vilenkin, "Gamma-ray bursts from superconducting cosmic strings," Phys. Rev. D **64**, 043004 (2001) [astro-ph/0102366];
K. S. Cheng, Y. -W. Yu and T. Harko, "High Redshift Gamma-Ray Bursts: Observational Signatures of Superconducting Cosmic Strings?," Phys. Rev. Lett. **104**, 241102 (2010) [arXiv:1005.3427 [astro-ph.HE]].

[25] R. H. Brandenberger and X. -m. Zhang, "Anomalous global strings and primordial magnetic fields," Phys. Rev. D **59**, 081301 (1999) [hep-ph/9808306].

[26] T. Vachaspati and A. Vilenkin, "Gravitational Radiation from Cosmic Strings," Phys. Rev. D **31**, 3052 (1985);
R. L. Davis, "Nucleosynthesis Problems for String Models of Galaxy Formation", Phys. Lett. **B 161**, 285 (1985).

[27] R. H. Brandenberger, A. Albrecht and N. Turok, "Gravitational Radiation From Cosmic Strings And The Microwave Background," Nucl. Phys. B **277**, 605

(1986).

[28] T. Damour and A. Vilenkin, "Gravitational radiation from cosmic (super)strings: Bursts, stochastic background, and observational windows," Phys. Rev. D **71**, 063510 (2005) [hep-th/0410222];
S. Olmez, V. Mandic and X. Siemens, "Gravitational-Wave Stochastic Background from Kinks and Cusps on Cosmic Strings," Phys. Rev. D **81**, 104028 (2010) [arXiv:1004.0890 [astro-ph.CO]].

[29] R. van Haasteren, Y. Levin, G. H. Janssen, K. Lazaridis, M. K. B. W. Stappers, G. Desvignes, M. B. Purver and A. G. Lyne *et al.*, "Placing limits on the stochastic gravitational-wave background using European Pulsar Timing Array data," arXiv:1103.0576 [astro-ph.CO].

[30] R. H. Brandenberger, "On The Decay Of Cosmic String Loops," Nucl. Phys. B **293**, 812 (1987).

[31] S. A. Sanidas, R. A. Battye and B. W. Stappers, "Constraints on cosmic string tension imposed by the limit on the stochastic gravitational wave background from the European Pulsar Timing Array," Phys. Rev. D **85**, 122003 (2012) [arXiv:1201.2419 [astro-ph.CO]].

[32] B. Shlaer, A. Vilenkin and A. Loeb, "Early structure formation from cosmic string loops," JCAP **1205**, 026 (2012) [arXiv:1202.1346 [astro-ph.CO]].

[33] R. Moessner and R. H. Brandenberger, "Formation of high redshift objects in a cosmic string theory with hot dark matter," Mon. Not. Roy. Astron. Soc. **280**, 797 (1996) [astro-ph/9510141].

[34] H. Tashiro, E. Sabancilar and T. Vachaspati, "Constraints on Superconducting Cosmic Strings from Early Reionization," Phys. Rev. D **85**, 123535 (2012) [arXiv:1204.3643 [astro-ph.CO]].

[35] K. D. Olum and A. Vilenkin, "Reionization from cosmic string loops," Phys. Rev. D **74**, 063516 (2006) [astro-ph/0605465].

[36] V. S. Berezinsky, V. I. Dokuchaev and Y. .N. Eroshenko, "Dense DM clumps seeded by cosmic string loops and DM annihilation," JCAP **1112**, 007 (2011) [arXiv:1107.2751 [astro-ph.HE]].

[37] R. Brandenberger, *Lectures on the Theory of Cosmological Perturbations,* 2003, [arXiv:hep-th/0306071].

[38] A.R. Liddle, D.H. Lyth, 2000, *Cosmological Inflation and Large-Scale Structure,* (Cambridge University Press, Cambridge)

[39] S. Weinberg, *Gravitation and Cosmology: Principles and Applications of the General Theory of Relativity*, 1972, (Wiley, New York)

[40] S. Dodelson, *Modern Cosmology*, 2003, Academic Press; 1 edition

[41] R. Barkana & A. Loeb *In the Beginning: The First Sources of Light and the Reionization of the Universe,* 2001, Phys. Rep. 349, 125-238

[42] G. Hinshaw et al., *Nine-Year Wilkinson Microwave Anisotropy Probe (WMAP) Observations: Cosmological Parameter Results*, 2012, [arXiv:1212.5226]

[43] T. Padmanabhan, *Structure Formation in the Universe*, 1993, (Cambridge University Press, Cambridge)

[44] J.R. Bond, S. Cole, G. Efstathiou, N. Kaiser, *Excursion set mass functions for hierarchical Gaussian fluctuations*, 1991, ApJ, 379, 440

[45] F. Bernardeau, S. Colombi, E. Gaztanaga, R. Scoccimarro, *Large-Scale Structure of the Universe and Cosmological Perturbation Theory*, 2002, PhysRep, 367, 1

[46] J.J.M. Carrasco, M.P. Hertzberg, L. Senatore, *The Effective Field Theory of Cosmological Large Scale Structures*, 2012, JHEP 1209, 082

[47] D. Reed, R. Bower, C. Frenk, A. Jenkins and T. Theuns, 2007 "The halo mass function from the dark ages through the present day," Mon. Not. Roy. Astron. Soc. **374**, 2 [astro-ph/0607150].

[48] R. K. Sheth, G. Tormen, *Large scale bias and the peak background split*,1999, Mon.Not.Roy.Astron.Soc. 308 119, arXiv:astro-ph/9901122 [astro-ph].

[49] A. H. Guth, *The Inflationary Universe: A Possible Solution to the Horizon and Flatness Problems*, 1981, Physical Review D23: 347

[50] J.P. Preskill, *Cosmological Production of Superheavy Magnetic Monopoles*, 1979, Phys. Rev. Lett. 43 (19): 1365
Y.B. Zeldovich, M.Y. Khlopov, *On the Concentration of Relic Magnetic Monopoles in the Universe*, 1978, Phys. Lett. B79 (3): 23941

[51] I. Chuang, R. Durrer, N. Turok, B. Yurke, *Cosmology in the Laboratory: Defect Dynamics in Liquid Crystals*, 1991, Science 251:13361342

[52] G.H. Derrick, *Comments on nonlinear wave equations as models for elementary particles*, 1964, J. Mathematical Phys. 5: 1252-1254.

[53] A. Vilenkin, E.P.S. Shellard, *Cosmic Strings and other Topological Defects,* 2000, 2nd edition (Cambridge University Press, Cambridge)

[54] D.P. Bennett, S.H. Rhie, *Cosmological evolution of global monopoles and the origin of large-scale structure*, 1990, Phys. Rev. Lett. 65, 1709

[55] T. W. B. Kibble, *Topology of Cosmic Domains and Strings,* 1976, J. Phys. A A 9, 1387

[56] T. W. B. Kibble, *Evolution of a system of cosmic strings,* 1985, Nucl. Phys. B252, 227

[57] V. Vanchurin, K. Olum, A. Vilenkin, *Cosmic string scaling in flat space*, Phys.Rev. D72 (2005) 063514

[58] X. Siemens, K. Olum, A. Vilenkin, *On the size of the smallest scales in cosmic string networks*, Phys.Rev. D66 (2002) 043501

[59] J.J. Blanco-Pillado, K.D. Olum, B. Shlaer, *Large parallel cosmic string simulations: New results on loop production*, Phys.Rev.D83:083514, 2011, [arXiv:1101.5173]

[60] E. Bertschinger, *Cosmological Accretion Wakes,* 1987, ApJ **316**, 489

[61] Y. .B. Zeldovich, *Gravitational instability: An Approximate theory for large density perturbations*, 1970, Astron. Astrophys. **5**, 84

[62] R. Brandenberger, R. J. Danos, O. F. Hernandez and G. P. Holder, *The 21 cm Signature of Cosmic String Wakes,* 2010, [arXiv:astro-ph/1006.2514v3].

[63] A. Sornborger, R. Brandenberger, B. Fryxell and K. Olson, *The Structure of Cosmic String Wakes,* ApJ $\mathbf{482 : 22 - 32}$, (1997).

[64] O. F. Hernandez, R. H. Brandenberger, *The 21 cm Signature of Shock Heated and Diffuse Cosmic String Wakes*, 2012, JCAP 1207, 032 [arXiv:1203.2307 [astro- ph.CO]].

[65] S. Furlanetto, S. P. Oh, F. Briggs, *Cosmology at Low Frequencies: The 21 cm Transition and the High-Redshift Universe*, 2006, Phys.Rept. 433, 181, [astro-ph/0608032].

[66] S.M. Miyama, S. Narita & C. Hayashi, *Fragmentation of Isothermal Sheet-Like Clouds. I,* Prog. Theor. Phys. **78** (1987), 1051.

[67] T. Hara and S. Miyoshi, *Formation Of The First Systems In The Wakes Of Moving Cosmic Strings,'* Prog. Theor. Phys. **77**, 1152 (1987).

[68] J. A. Fillmore and P. Goldreich, *Self-similiar gravitational collapse in an expanding universe,'* Astrophys. J. **281**, 1 (1984).

[69] P. Scott, S. Sivertsson, *Gamma-Rays from Ultracompact Primordial Dark Matter Minihalos*, 2009, Phys.Rev.Lett. 103 211301, [arXiv:0908.4082].

[70] L. Perivolaropoulos, *COBE versus cosmic strings: An Analytical model,'* Phys. Lett. B **298**, 305 (1993) [arXiv:hep-ph/9208247];

[71] O. F. Hernandez, Y. Wang, R. Brandenberger, and J. Fong, *Angular 21 cm Power Spectrum of a Scaling Distribution of Cosmic String Wakes,* 2011, [arXiv:astro-ph/1104.3337v2].

[72] H. Hoekstra & B. Jain *Weak Gravitational Lensing and its Cosmological Applications,* Ann.Rev.Nucl.Part.Sci.58:99-123,2008 , [arXiv:0805.0139v1].

[73] M. Bartelmann & P. Schneider, *Weak gravitational lensing,* Physics Reports 340 (2001) 291472, [astro-ph/9912508].

[74] E. Zackrisson & T. Riehm, *Gravitational lensing as a probe of cold dark matter subhalos*, 2009, [arXiv:0905.4075].

[75] E. Zackrisson, S. Asadi, K. Wiik, J. Jnsson, P. Scott, K.K. Datta, M.M. Friedrich, H. Jensen, J. Johansson, C. Rydberg & A. Sandberg, *Hunting for dark halo substructure using submilliarcsecond-scale observations of macrolensed radio jets*, 2012, [arXiv:1208.5482].

[76] D.D. Xu, S. Mao, A. Cooper, L. Gao, C. S. Frenk, R.E. Angulo & J. Helly , *On the effects of line-of-sight structures on lensing flux-ratio anomalies in a ΛCDM universe* 2012, MNRAS, 421, 2553, [arXiv1110.1185].

[77] http://masterlens.astro.utah.edu

[78] K. R. Mecke, T. Buchert, H. Wagner, *Robust morphological measures for large scale structure in the universe,'* Astron. Astrophys. **288**, 697-704 (1994). [astro-ph/9312028];

J. Schmalzing, M. Kerscher, T. Buchert, *Minkowski functionals in cosmology*, arXiv:astro-ph/9508154.

C. Hikage, J. Schmalzing, T. Buchert, et al., *Minkowski Functionals of SDSS galaxies I : Analysis of Excursion Sets*, 2003, PASJ, 55, 911, [arXiv:astro-ph/0304455]

[79] J. Schmalzing and T. Buchert, *Beyond genus statistics: a unifying approach to the morphology of cosmic structure,'* Astrophys. J. **482**, L1 (1997) [arXiv:astro-ph/9702130].

[80] H. Hadwiger, Vorlesungen uber Inhalt, Oberflache und Isoperimetrie (Springer, Berlin, 1957).

[81] M. Boylan-Kolchin et al., *Resolving Cosmic Structure Formation with the Millennium-II Simulation,* 2009, MNRAS 398, 1150, arXiv:0903.3041

[82] R. H. Brandenberger, R. J. Danos, O. F. Hernandez and G. P. Holder, "The 21 cm Signature of Cosmic String Wakes," JCAP **1012**, 028 (2010) [arXiv:1006.2514 [astro-ph.CO]].

[83] E. McDonough and R. H. Brandenberger, "Searching for Signatures of Cosmic String Wakes in 21cm Redshift Surveys using Minkowski Functionals," arXiv:1109.2627 [astro-ph.CO].

[84] O. F. Hernandez and R. H. Brandenberger, "The 21 cm Signature of Shock Heated and Diffuse Cosmic String Wakes," JCAP **1207**, 032 (2012) [arXiv:1203.2307 [astro-ph.CO]].

[85] M. Pagano and R. Brandenberger, "The 21cm Signature of a Cosmic String Loop," JCAP **1205**, 014 (2012) [arXiv:1201.5695 [astro-ph.CO]].